Dalton Transactions

ROYAL SOCIETY OF CHEMISTRY

PAPER

View Article Online
View Journal | View Issue

Cite this: *Dalton Trans.*, 2024, **53**, 8463

Unveiling the promising anticancer activity of palladium(II)–aryl complexes bearing diphosphine ligands: a structure–activity relationship analysis†

Giovanni Tonon, [a] Matteo Mauceri,[a] Enrico Cavarzerani,[a] Rachele Piccolo,[a] Claudio Santo,[a] Nicola Demitri, [b] Laura Orian, [c] Pablo A. Nogara, [d] João Batista T. Rocha, [d] Vincenzo Canzonieri, [e,f] Flavio Rizzolio, *[a,e] Fabiano Visentin *[a] and Thomas Scattolin *[c]

In continuation of our previous works on the cytotoxic properties of organopalladium compounds, in this contribution we describe the first systematic study of the anticancer activity of Pd(II)–aryl complexes. To this end, we have prepared and thoroughly characterized a wide range of palladium derivatives bearing different diphosphine, aryl and halide ligands, developing, when necessary, specific synthetic protocols. Most of the synthesized compounds showed remarkable cytotoxicity towards ovarian and breast cancer cell lines, with IC_{50} values often comparable to or lower than that of cisplatin. The most promising complexes ([PdI(Ph)(dppe)] and [PdI(*p*-CH_3-Ph)(dppe)]), characterized by a diphosphine ligand with a low bite angle, exhibited, in addition to excellent cytotoxicity towards cancer cells, low activity on normal cells (MRC5 human lung fibroblasts). Specific immunofluorescence tests (cytochrome c and H2AX assays), performed to clarify the possible mechanism of action of this class of organopalladium derivatives, seemed to indicate DNA as the primary cellular target, whereas caspase 3/7 assays proved that the complex [PdI(Ph)(dppe)] was able to promote intrinsic apoptotic cell death. A detailed molecular docking analysis confirmed the importance of a diphosphine ligand with a reduced bite angle to ensure a strong DNA–complex interaction. Finally, one of the most promising complexes was tested towards patient-derived organoids, showing promising *ex vivo* cytotoxicity.

Received 28th March 2024,
Accepted 17th April 2024

DOI: 10.1039/d4dt00919c

rsc.li/dalton

Introduction

Palladium(II)–aryl complexes represent a fascinating and important class of organometallic compounds that have found extensive applications in the field of homogeneous catalysis.[1–19] These palladium compounds are also valuable synthons in organometallic chemistry, enabling the formation of novel organopalladium derivatives with interesting properties.[20–23] Beyond their synthetic applications, Pd(II)–aryl derivatives have found utility in the field of materials science. For instance, they are employed in the fabrication of organic light-emitting diodes (OLEDs) and other electronic devices.[24,25] In addition, the ability to precisely control the arrangement of aryl groups through Pd-catalyzed processes enables the fine-tuning of the electronic and optical properties of these materials.

As far as the application of Pd(II)–aryl complexes in medicinal chemistry is concerned, it is curious to note that, excluding studies on cyclopalladates[26] and a couple of contributions dealing with Pd(II) complexes bearing perfluorinated aryl ligands,[27,28] no systematic study on the antitumor activity of Pd(II) complexes with classical monodentate aryl fragments is found in the literature.

For this reason, with the aim of filling this gap and encouraged by some recent studies conducted on the promising anticancer activity of organopalladium compounds,[29–36] in this work we propose the synthesis and study of the antiprolifera-

[a]*Dipartimento di Scienze Molecolari e Nanosistemi, Università Ca' Foscari, Campus Scientifico Via Torino 155, 30174 Venezia-Mestre, Italy. E-mail: fvise@unive.it, flavio.rizzolio@unive.it*
[b]*Elettra – Sincrotrone Trieste, S.S. 14 Km 163.5 in Area Science Park, 34149 Basovizza, Trieste, Italy*
[c]*Dipartimento di Scienze Chimiche, Università degli Studi di Padova, via Marzolo 1, 35131 Padova, Italy. E-mail: thomas.scattolin@unipd.it*
[d]*Departamento de Bioquímica e Biologia Molecular, Centro de Ciências Naturais e Exatas, Universidade Federal de Santa Maria, Santa Maria, RS, Brazil*
[e]*Pathology Unit, Centro di Riferimento Oncologico di Aviano (C.R.O.) IRCCSvia Franco Gallini 2, 33081 Aviano, Italy. E-mail: flavio.rizzolio@unive.it*
[f]*Department of Medical, Surgical and Health Sciences, Università degli Studi di Trieste, Strada di Fiume 447, Trieste, Italy*

†Electronic supplementary information (ESI) available. CCDC 2324438–2324443. For ESI and crystallographic data in CIF or other electronic formats see DOI: https://doi.org/10.1039/d4dt00919c

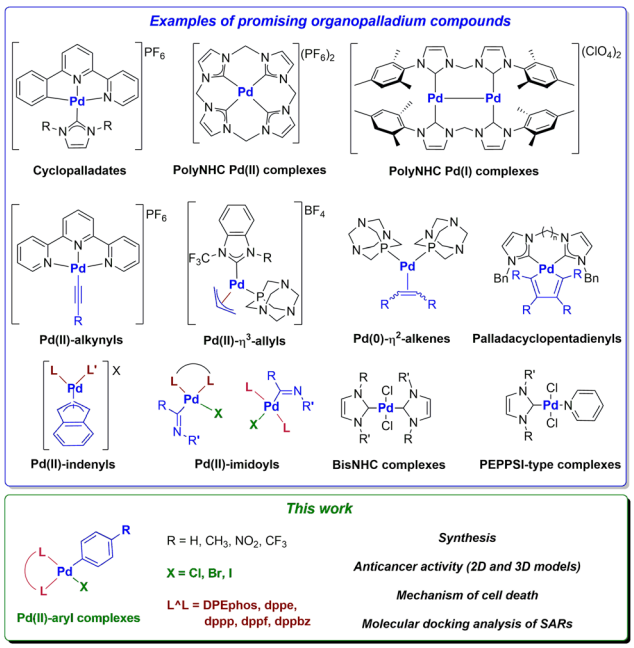

Fig. 1 Relevant examples of organopalladium compounds with promising anticancer activity and target complexes of this work.[29]

tive activity of Pd(II)–aryl complexes bearing diphosphine ancillary ligands (Fig. 1). *In vitro* tests on ovarian and breast cancer cell lines allowed us to select one of the most promising complexes and to carry out a preliminary study on its mechanism of action, as well as to determine its cytotoxicity on patient-derived organoids. Finally, considering the biotarget identified for this important class of organopalladium compounds, we propose a structure–activity relationship (SAR) analysis using a molecular docking approach. This method allows us to evaluate, in a qualitative and intuitive way, the influence of each ligand bonded to palladium on the antitumor activity observed *in vitro*.

Results and discussion

Synthesis of Pd(II)–aryl complexes

Most of the Pd(II)–aryl complexes used in this work were synthesized through the ligand exchange reaction between [PdI(tmeda)(*p*-R-Ph)] precursors **1a–d** (tmeda = *N*,*N*,*N*′,*N*′-tetramethylethylenediamine; R = H, CH_3, CF_3, NO_2) and five different diphosphine ligands (dppe = 1,2-bis(diphenylphosphino)ethane, dppp = 1,2-bis(diphenylphosphino)propane, dppf = 1,1′-bis(diphenylphosphino)ferrocene, dppbz = 1,2-bis(diphenylphosphino)benzene and DPEphos = bis[(2-diphenylphosphino)phenyl] ether). While the diphosphines are all commercially available, the [PdI(tmeda)(*p*-R-Ph)] precursors **1a–d** were instead prepared according to the protocol reported in the literature.[21,22]

Following a slightly modified procedure with respect to that described by Hartwig and colleagues,[21] substitution of the tmeda ligand with the selected diphosphines occurred at room temperature in a few minutes, using anhydrous dichloromethane as a solvent. The only exception is complexes containing dppbz (**5a–b**), for which the exchange reaction is definitely slower and is completed within 1 hour. A more detailed kinetic study of this process is reported in the ESI.†

Scheme 1 shows the general reaction for the synthesis of the target complexes and the yields obtained. It should be noted that not all aryl fragment/diphosphine ligand combinations led to the isolation of the complexes of interest with sufficient purity. For this reason, only the compounds obtained in a pure form are reported in Scheme 1.

While complexes **2b–d**, **3a** and **4b–d** were previously reported by other research groups,[21,37–40] six of the synthesized complexes ([PdI(*p*-NO_2-Ph)(dppf)] **4a**, [PdI(*p*-NO_2-Ph)(dppe)] **2a**, [PdI(*p*-NO_2-Ph)(dppbz)] **5a**, [PdI(*p*-NO_2-Ph)(DPEphos)] **6a**, [PdI(*p*-CF_3-Ph)(dppbz)] **5b** and [PdI(*p*-CF_3-Ph)(DPEphos)] **6b**) have never been published before. Therefore, these derivatives were exhaustively characterized by ^{1}H, ^{31}P, ^{19}F, ^{13}C NMR and FT-IR spectroscopy (Fig. S1–65 in ESI†). Moreover, in the case of complexes **4a** and **6a**, it was possible to unequivocally confirm their structure by XRD analysis of suitable crystals obtained by slow evaporation of diethyl ether in a dichloromethane solution of the Pd(II) complex (Fig. 2). Conversely, the correct outcome of the synthesis of the Pd(II)–aryl derivatives already reported in the literature was confirmed by ^{1}H, ^{31}P and ^{19}F NMR analyses.[21,37–40]

Going into more detail about the characterization of the synthesized complexes, in all ^{1}H NMR spectra the disappearance of the peaks of coordinated tmeda and the appearance of the peaks of the aromatic and aliphatic protons of the coordinated diphosphine are detectable. These latter signals are shifted and doubled compared to those of the free diphosphine, due to the presence of two different ligands in the Pd(II) coordination sphere (iodide and aryl fragment). Coordination of the chelating diphosphine is confirmed by the ^{31}P NMR spectra, in which it is possible to observe the presence of two doublets, caused by the coupling of the two non-equivalent phosphorus nuclei, localised at higher chemical shifts compared to the singlet observable in the case of the free diphosphine. This shift is attributable to the strong

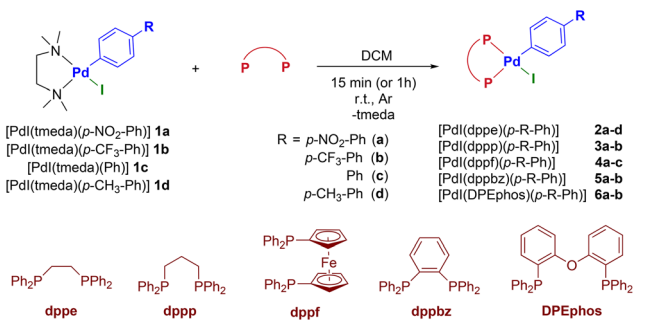

Scheme 1 Synthetic procedure to target Pd(II)–aryl complexes.

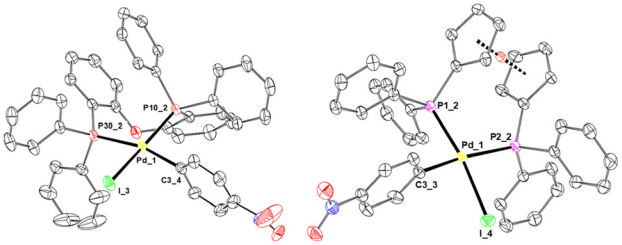

Fig. 2 X-ray molecular structures of **4a** (right) and **6a** (left) are presented, showing thermal displacement ellipsoids at the 50% probability level with hydrogen atoms and solvent molecules omitted for clarity.

σ-donor character of the diphosphines used and their coordination on the metal centre.

With the aim of evaluating not only the effect of the aryl and diphosphine fragments, but also the role of the halide ligand on the cytotoxicity of the target complexes, we wondered which could be the most promising synthetic route to Pd(II)–aryl complexes bearing chloride and bromide ligands.

After some preliminary tests we chose to prepare a Pd(II) precursor bearing 8-(*tert*-butylthio)quinoline (TtBQ) as an ancillary ligand. More precisely, we opted for [PdI(TtBQ)(*p*-NO_2-Ph)] (**7-I**) as a model compound.[41]

Based on studies previously conducted by our group, the presence of an N^S ancillary ligand such as thioquinoline derivatives, enables the replacement of the iodide ligand with a bromide or a chloride by the simple addition of a stoichiometric amount of IBr or ICl, respectively.[42] This reaction is particularly interesting as it avoids the use of silver-based dehalogenating agents, which are light-sensitive and often difficult to remove completely. In addition, the cationic intermediates that form before the entry of the new halide are generally not very stable, leading to very low yields or even preventing the isolation of the product of interest.

However, it is important to point out that the halide metathesis carried out with IBr or ICl is selective only in the case of Pd(II) complexes bearing N^S ligands.[42] In fact, when P^P ligands are used, the same process leads to mixtures of products, the identities of which are difficult to establish.

Gratifyingly, the addition of IBr or ICl to complex **7-I** allowed us to synthesize complexes [PdBr(TtBQ)(*p*-NO_2-Ph)] (**7-Br**) and [PdCl(TtBQ)(*p*-NO_2-Ph)] (**7-Cl**), respectively, in high yields and purity (see Scheme 2).

These complexes have been characterized by ^{1}H, ^{13}C NMR, and IR spectroscopy. For example, in the case of complex [PdCl(*p*-NO_2-Ph)(TtBQ)] (**7-Cl**) it is possible to detect one singlet at 1.23 ppm ascribable to *tert*-butyl protons and one multiplet at 7.68–7.80 ppm attributable to H^3, H^6 quinoline protons and two of the phenyl protons. A further multiplet in the 7.86–7.91 region is attributable to the two remaining phenyl protons. H^7 and H^5 appear in the form of two very close doublets of doublets, located at 8.08 ppm (J = 7.5 Hz, 1.3 Hz) and 8.11 ppm (J = 8.4 Hz, 1.3 Hz), while H^4 generates a doublet of doublets (J = 8.4 Hz, 1.6 Hz) at 8.46 ppm.

Finally, the most diagnostic signal corresponds to H^2 (9.78 ppm, dd, J = 4.9 Hz, 1.6 Hz), which confirms the presence of the chloride ligand. In fact, this signal is present at 9.95 and 10.12 ppm in the complexes [PdBr(*p*-NO_2-Ph)(TtBQ)] (**7-Br**) and [PdI(*p*-NO_2-Ph)(TtBQ)] (**7-I**), respectively.

To further confirm halide metathesis, it was possible to obtain the structure of complexes **7-Cl** and **7-Br** by means of XRD analysis (Fig. 3). It is interesting to note that between the two possible isomers, the isolated complexes are always characterized by the sulfur atom in the *trans* position with respect to the halide ligand. This behavior can be justified by the different *trans*-influences of the ligands. In fact, the aryl fragment is positioned *trans* with respect to the less *trans*-labilizing ligand of the thioquinoline ligand (nitrogen atom).

The thioquinoline ligand used (TtBQ) has the further advantage of being sufficiently labile to be replaced by diphosphine ligands. In particular, using dppf as a model ligand, complexes [PdBr(dppf)(*p*-NO_2-Ph)] (**4a-Br**) and [PdCl(dppf)(*p*-NO_2-Ph)] (**4a-Cl**) were synthesized (Scheme 3), and constitute the bromide and chloride congeners of complex [PdI(dppf)(*p*-NO_2-Ph)] (**4a**), the synthesis of which was discussed at the beginning of this section.

The identity of both complexes was ascertained by careful analysis of their ^{1}H, ^{31}P, ^{13}C NMR and IR spectra. As far as the ^{1}H NMR spectra are concerned, they obviously do not show substantial differences compared to that of complex [PdI(dppf)(*p*-NO_2-Ph)] (**4a**) in terms of the number and multiplicity of signals. However, significant differences are observed concerning the chemical shifts of some peaks.

As regards the ^{31}P NMR spectra, a general trend is observed for both phosphorus signals: as the electronegativity of the halogen increases, the signals relating to the phosphorus nuclei shift to higher chemical shifts. In fact, chloride exerts a lower *trans*-influence than iodide and this involves greater electron donation by the phosphorus of the phosphine, with the consequent shift to higher chemical shifts of the signal relating to the phosphorus nucleus *trans* with respect to the halide. Notably, in

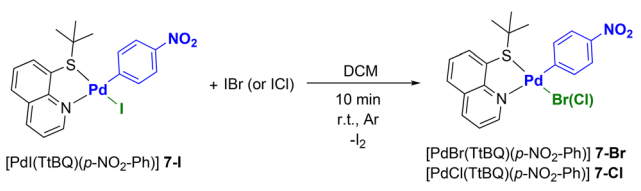

[PdI(TtBQ)(*p*-NO_2-Ph)] **7-I**

[PdBr(TtBQ)(*p*-NO_2-Ph)] **7-Br**
[PdCl(TtBQ)(*p*-NO_2-Ph)] **7-Cl**

Scheme 2 Halide-metathesis reactions.

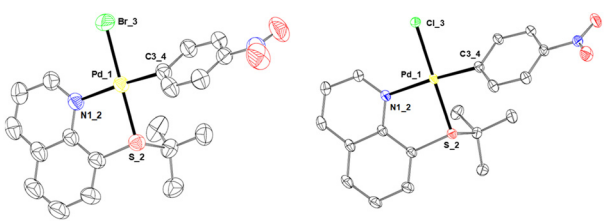

Fig. 3 X-ray molecular structures of **7-Cl** (right) and **7-Br** (left) are presented, showing thermal displacement ellipsoids at the 50% probability level with hydrogen atoms and solvent molecules omitted for clarity.

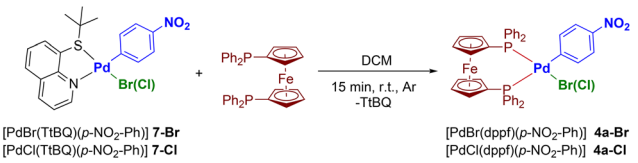

Scheme 3 Synthetic procedure for Pd(II)–aryl complexes bearing dppf and bromide (or chloride) ligands.

the case of complexes **4a-Cl** and **4a-Br** it was possible to confirm the proposed structures by XRD analysis (Fig. 4).

Spectroscopic data for the synthesized Pd(II)–aryl complexes are summarized in Table S8 of the ESI.†

Structural characterization of Pd(II)–aryl complexes

Complexes **7-Br**, **7-Cl**, **4a**, **4a-Br**, **4a-Cl** and **6a** have been crystallized, characterized through XRD and show square planar Pd (II) coordination spheres (Tables S1–7 in ESI†). A change of the chelating ligand has an impact on the Pd(II)–C bond. Lengthening of the Pd–C bond is found when the phosphine is in the *trans*-position, reflecting the different electronic properties of P and N atoms. Minor differences can be observed as a consequence of halogen substitutions.

All the crystalline forms bear one crystallographically independent neutral Pd(II) complex each. A comparison of phosphine-based complexes (**4a**, **4a-Br**, **4a-Cl** and **6a**) shows almost perfectly superimposable atomic positions (Fig. S70 in ESI† – R.M.S.D. < 0.6 Å). Replacement of pentacene is efficiently compensated for by proper phosphine phenyl ring stacking in **6a** ($d_{\pi-\pi}$ = 3.627(2) Å between ring centroids with 0.79 Å slippage). Identical conformations are also found for the thioquinoline derivatives **7-Br** and **7-Cl** (Fig. S71 in ESI† – R.M.S.D. ~0.1 Å). Crystal packing shows hydrophobic contacts among neighbouring molecules, involving weak intermolecular π···π and CH···π interactions, among neighbouring aromatic rings. Solvent molecules were found in the crystal packing of **6a** (*i.e.* heavily disordered dichloromethane and diethyl ether).

Antiproliferative activity on human cancer and normal cell lines

With the aim of investigating the potential anticancer activity of our Pd(II)–aryl complexes, a panel of four different human tumor cell lines (ovarian cancer A2780, with its cisplatin resistant clone A2780*cis*, high-grade serous ovarian cancer OVCAR-5 and triple-negative breast cancer MDA-MB231) and MRC-5 normal cells (human lung fibroblasts) were treated for 96 hours with the synthesized compounds and cisplatin (positive control).

Importantly, all the synthesized complexes are soluble when the DMSO stock solution (2.5 mM) is diluted in the culture medium to final concentrations of 100 μM, 10 μM, 1 μM, 0.1 μM, 0.01 μM, and 0.001 μM.

In the preliminary phase, we monitored the stability of the Pd (II)–aryl complexes in a 1 : 1 D_2O/DMSO-d_6 solution by NMR spectroscopy. After 24 hours no significant changes to the spectra are detectable, indicating that the complexes retain their structural integrity. Particularly diagnostic are the peaks in the ^{31}P NMR spectra, which are almost superimposable on those recorded in chlorinated solvents (see Fig. S54 in ESI†). This aspect suggests that the hydrolysis of the Pd(II)–halide bond does not occur, as the formation of aquo species would lead to a significant change in the ^{31}P NMR spectra. The only exception is complex [PdI(*p*-CH_3-Ph)(dppf)] (**4d**), which decomposes rapidly under such conditions and was therefore not considered for biological tests.

The antiproliferative activity results for the tested compounds are reported in Table 1 in terms of half inhibitory concentrations (IC_{50}) values.

On the basis of these IC_{50} values it is possible to draw some interesting conclusions.

As far as the A2780 and A2780*cis* cell lines (cisplatin-sensitive and cisplatin-resistant ovarian cancer, respectively) are concerned, the IC_{50} values fall in the low micromolar range and there are no marked differences between the tested compounds. It seems that among the complexes with the formula [PdX(*p*-NO_2-Ph)(dppf)] (X = Cl, Br, I), the most active derivative is that with a chloride ligand. As regards the effect of the group in the *para* position of the aryl fragment, no significant trends are observed in the two lines. In the A2780 cell line, all compounds exhibit a cytotoxicity comparable with that of cisplatin, with the exception of complex [PdI(*p*-NO_2-Ph)(dppbz)] (**5a**), for which it is more than an order of magnitude lower. Interestingly, in the cisplatin-resistant ovarian cancer cell line (A2780*cis*), all compounds are more active than cisplatin by up to an order of magnitude. Given that the IC_{50} values obtained on the A2780 and A2780*cis* cell lines are comparable in all tested compounds, while those of cisplatin differ by an order of magnitude (1.1 μM *vs.* 11 μM), we can reasonably assume that the mechanism of action of our complexes is different from that of platinum-based drugs.

In the OVCAR-5 (high-grade serous ovarian cancer) cell line, most compounds exhibit higher IC_{50} values with respect to those obtained on the A2780 cell line. In particular, some complexes were found to be substantially inactive (IC_{50} > 100, **2a**, **4a**, **4a-Cl**, **4a-Br** and **6a–b**), others were active but much less than cisplatin (**4b** and **5a**), while some were comparable with the reference drug (**2b–d**, **3a–b**, **4c** and **5b**). The latter complexes are mostly characterized by the presence of diphosphine ligands with a reduced bite angle (dppe, dppp and dppbz).

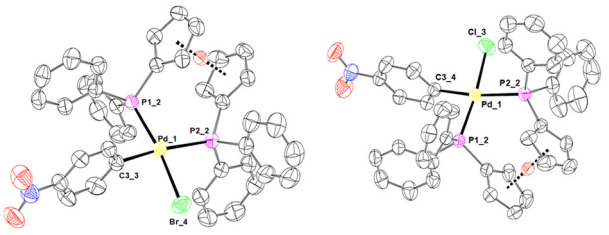

Fig. 4 X-ray molecular structures of **4a-Cl** (right) and **4a-Br** (left) are presented, showing thermal displacement ellipsoids at the 50% probability level with hydrogen atoms and solvent molecules omitted for clarity.

Table 1 Antiproliferative activity on the A2780, A2780cis, OVCAR-5, MDA-MB-231 and MRC-5 cell lines

	IC_{50} (μM)				
Compound	A2780	A2780*cis*	OVCAR-5	MDA-MB-231	MRC-5
Cisplatin	**1.1 ± 0.1**	**11 ± 3**	**2 ± 1**	**28 ± 3**	**3.9 ± 0.6**
[PdI(*p*-NO_2-Ph)(dppe)] (**2a**)	4.1 ± 0.4	3.3 ± 0.2	>100	7 ± 1	>100
[PdI(*p*-CF_3-Ph)(dppe)] (**2b**)	3.26 ± 0.04	3.0 ± 0.5	10 ± 2	3 ± 1	19 ± 2
[PdI(Ph)(dppe)] (**2c**)	3.1 ± 0.2	5 ± 1	5 ± 1	4.7 ± 0.4	>100
[PdI(*p*-CH_3-Ph)(dppe)] (**2d**)	1.8 ± 0.3	7 ± 1	6 ± 1	2 ± 1	>100
[PdI(*p*-NO_2-Ph)(dppp)] (**3a**)	3.1 ± 0.8	2.9 ± 0.7	2.4 ± 0.1	3 ± 1	5.4 ± 0.5
[PdI(*p*-CF_3-Ph)(dppp)] (**3b**)	3.8 ± 0.2	3.1 ± 0.5	8.0 ± 0.4	4 ± 1	4.1 ± 0.2
[PdI(*p*-NO_2-Ph)(dppf)] (**4a**)	8 ± 1	3.5 ± 0.4	>100	22 ± 4	>100
[PdBr(*p*-NO_2-Ph)(dppf)] (**4a-Br**)	4.6 ± 0.5	3.1 ± 0.2	>100	30 ± 10	>100
[PdCl(*p*-NO_2-Ph)(dppf)] (**4a-Cl**)	2.7 ± 0.3	1.5 ± 0.3	>100	90 ± 50	>100
[PdI(*p*-CF_3-Ph)(dppf)] (**4b**)	14 ± 3	4.3 ± 0.6	40 ± 7	11 ± 2	>100
[PdI(Ph)(dppf)] (**4c**)	2.1 ± 0.3	1.4 ± 0.3	6.6 ± 0.4	5 ± 1	3.2 ± 0.3
[PdI(*p*-NO_2-Ph)(dppbz)] (**5a**)	17 ± 2	6 ± 1	40 ± 20	>100	>100
[PdI(*p*-CF_3-Ph)(dppbz)] (**5b**)	3.9 ± 0.2	4.2 ± 0.4	12 ± 1	4 ± 1	4.26 ± 0.05
[PdI(*p*-NO_2-Ph)(DPEphos)] (**6a**)	7.5 ± 0.7	1.0 ± 0.2	>100	10 ± 3	>100
[PdI(*p*-CF_3-Ph)(DPEphos)] (**6b**)	3.1 ± 0.4	0.8 ± 0.1	>100	>100	>100

Data after 96 h of incubation. Stock solutions in DMSO for all complexes; stock solutions in H_2O for cisplatin. A2780 (cisplatin-sensitive ovarian cancer cells), A2780*cis* (cisplatin-resistant ovarian cancer cells), OVCAR-5 (high-grade serous ovarian cancer cells), MDA-MB-231 (triple-negative breast cancer), MRC-5 (normal lung fibroblasts).

Even in the triple-negative breast cancer cell line (MDA-MB-231), most of the compounds tested that exhibited a remarkable cytotoxicity (up to an order of magnitude higher than cisplatin) are those bearing diphosphine ancillary ligands with a low bite angle. Notably, the three complexes that are inactive against this type of cancer cell (**4a-Cl**, **5a** and **6b**) are characterized by the presence of DPEphos, dppbz and dppf diphosphines, and aryl ligands with electron-withdrawing substituents. Contrary to the trend observed for the A2780 and A2780*cis* cell lines, it seems that among the compounds with the formula [PdX(*p*-NO_2-Ph)(dppf)], the most active are those bearing an iodide ligand.

In the case of the MRC-5 non-tumor cell line, cisplatin shows a very low IC_{50} (3.9 μM), which is substantially comparable to the results obtained on the four cancer cell lines, thus confirming the poor selectivity of this reference drug. Conversely, most of our complexes are inactive (IC_{50} > 100 μM) towards these normal cells, thus indicating a certain *in vitro* selectivity. This interesting result was not observed in the case of complexes **2b**, **3a–b**, **4c** and **5b**.

Overall, the most promising complexes are those that are active on all tumor cell lines investigated and, at the same time, inactive towards non-tumor cells (MRC-5). Among all the compounds tested, **2c** and **2d** are the only ones that fully satisfy these characteristics. Complex [PdI(*p*-CF_3-Ph)(dppf)] (**4b**) is also quite promising, even if it exhibits a relatively low cytotoxicity on the OVCAR-5 line (IC_{50} = 40 ± 7 μM). The two most interesting complexes (**2c** and **2d**) are characterized by the presence of a phosphine with a low bite angle (dppe) and by electron-rich aryl fragments (phenyl or *para*-tolyl).

Antiproliferative activity on patient-derived organoids

Encouraged by the results obtained on ovarian cancer cell lines, we envisioned whether further experiments on more complex biological models could furnish us with significant insights into the real efficacy of the compounds synthesized in this study. Within this framework, organoids are lab-built mini-organs that can act as models to summarise cancer development.[43] The emergence of innovative organoid biobanks represents the forefront of *ex vivo* drug testing.[44] Indeed, both innate and acquired chemoresistance, coupled with tumor heterogeneity, stand as formidable barriers to therapeutic success for ovarian cancer, necessitating innovative preclinical models to simulate this complexity.[45]

A few pioneering groups in this field are actively developing animal and *ex vivo* organoid models of ovarian cancer to more accurately replicate the responses observed in clinical patients.[46] It is crucial to remember that within the spectrum of ovarian cancers, the high-grade serous subtype (HGSOC) prevails as the most common and provides the lowest five-year survival rate.[45] Furthermore, approximately 30% of HGSOC patients develop ascites, comprising free-floating cells accountable for intraperitoneal metastasis.[47] Such patients pose challenges for conventional chemotherapy, often resorting to paracentesis for symptom relief.[48]

Given these challenges, existing lines of therapy are not effective, underscoring the pressing need for novel drugs to surmount innate or acquired resistance, which diminishes treatment effectiveness and, in turn, amplifies toxicity levels. Therefore, taking advantage of organoid biotechnology, we selected two patient-derived tumoroids (PDTO-1 and PDTO-2), originating from high-grade serous ovarian cancer (HGSOC) and recently isolated and characterized by our research group.[49] Notably, from immunohistochemistry (IHC) analyses, the established organoids captured the histological characteristics of the primary tumors. In particular, hematoxylin as well as PAX8, WT-1, and CA-125 HGOC markers were evaluated by the pathologist.

Table 2 Anticancer activity on patient-derived organoids

	IC_{50} (μM)	
Compound	PTDO-1	PTDO-2
Carboplatin	8 ± 2	9 ± 4
2c	37 ± 9	20 ± 9

The selected organoids were chosen to evaluate the effectiveness of one of the most promising Pd(II)–aryl complexes reported in this work (**2c**). The IC_{50} values reported in Table 2 demonstrate that complex **2c** exhibits good/moderate activity even in these more complex biological models. In more detail, the cytotoxicity of complex **2c** is comparable (same order of magnitude) to that of carboplatin, which is the reference compound for standard clinical therapy.

Mechanism of cell death

With the aim of determining the main biological target of the Pd(II)–aryl complexes reported in this work, we carried out a detailed study on OVCAR-5 cells using immunofluorescence techniques and [PdI(Ph)(dppe)] (**2c**) as a model compound.

Based on our experience from studying the mechanism of action of organopalladium compounds, we preliminarily investigated cytochrome c release, DNA damage and the activation of caspases 3/7. To strengthen the data, the biological experiments were conducted by a kinetic analysis at different timepoints.

We initially wondered whether our Pd(II)–aryl complexes could cause early mitochondrial damage to tumor cells. To this end, we first investigated the release of cytochrome c. The cytochrome c immunofluorescence assay is widely utilized in cell biology to investigate the subcellular localization and dynamics of cytochrome c within cells.[50] It should be remembered that cytochrome c is a crucial component of the mitochondrial electron transport chain and is involved in cellular respiration. However, during programmed cell death such as apoptosis, cytochrome c is released from the mitochondria into the cytoplasm. Alterations in cytochrome c distribution can function as an indicator of mitochondrial dysfunction and cellular death mechanisms, making this assay indispensable in research concerning apoptosis and mitochondrial activity. Following a well-established protocol, OVCAR-5 cells were treated with **2c** (5 and 10 μM) and cisplatin (10 μM as positive control) for 6, 24 and 48 hours.

The collected images showed the release of cytochrome c in the case of cisplatin after 6 hours, although it was more evident at 24 and 48 hours, thus confirming an apoptosis pathway for this clinical drug (Fig. 5). In the case of complex [PdI(Ph)(dppe)] (**2c**), a significant release of cytochrome c was detected after 24 and 48 hours at both concentrations (5 μM and 10 μM).

Following this assay, our attention turned towards examining DNA damage through the γH2AX immunofluorescence assay. The gamma H2AX assay specifically focuses on the phosphorylation of histone H2AX at serine 139 in response to

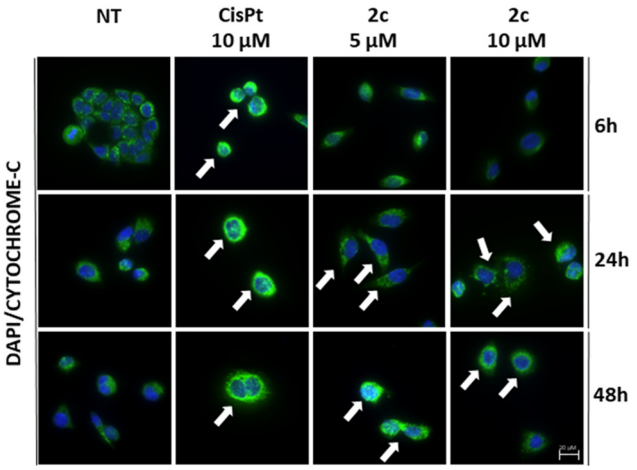

Fig. 5 Immunofluorescence analysis of cytochrome c release after 6, 24 and 48 h of treatment with complex **2c**. OVCAR-5 cancer cells were treated with complex **2c** at concentrations of 5 and 10 μM. Arrows indicate cytochrome c release. Positive control: cisplatin 10 μM. Magnification 100×, scale bar 20 μm.

double-strand breaks (DSBs) in the DNA molecule.[51] The term "gamma" refers to the gamma isoform of H2AX, which is a subtype of the histone H2A family. The gamma H2AX assay provides a sensitive and quantitative measure of DSBs, allowing researchers to evaluate the extent of DNA damage and the effectiveness of DNA repair mechanisms.[52]

One of the significant advantages of the gamma H2AX assay is its sensitivity. Even low levels of DNA damage can be detected, making it an invaluable tool for assessing the impact of various genotoxic agents.

As shown in Fig. 6, the cells treated with compound **2c** showed a marked phosphorylation of Ser139 of histone H2AX after 6, 24 and 48 hours. This result suggests that DNA is likely to be a major molecular target of our Pd(II)–aryl complexes. Notably, even in the case of cisplatin the phosphorylation of histone H2AX is clearly evident, thus confirming the well-known interaction between cisplatin and DNA (DNA platination).

Finally, we investigated the activation of caspases 3 and 7 to verify whether tumor cell death followed an apoptotic pathway. As a matter of fact, the caspases 3/7 assay is a well-established method in cell biology to assess apoptosis, a programmed cell death process crucial for maintaining tissue homeostasis and eliminating damaged or unwanted cells.[53] Caspases 3 and 7 are key executioner caspases that play a central role in the execution phase of apoptosis by cleaving various cellular substrates, leading to cell dismantling.

The obtained data (Fig. 7) show a marked activation of caspases 3 and 7 for both cisplatin (24 and 48 hours) and complex **2c** (at all timepoints with a 10 μM concentration).

These results suggest that in the case of complex **2c**, cell death follows an intrinsic apoptotic pathway.

Molecular docking analysis of structure–activity relationships

Aiming at better understanding the interaction between the Pd(II)–aryl complexes and DNA, molecular docking simulations

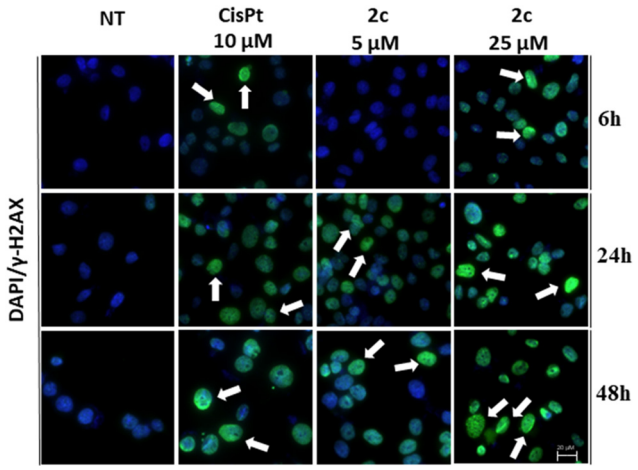

Fig. 6 Assay on DNA damage after 6, 24 and 48 h of treatment with complex **2c**. OVCAR-5 cancer cells were treated with complex **2c** at concentrations of 5 and 25 μM. Arrows indicate DNA damage. Positive control: cisplatin 10 μM. Magnification 100×, scale bar 20 μm.

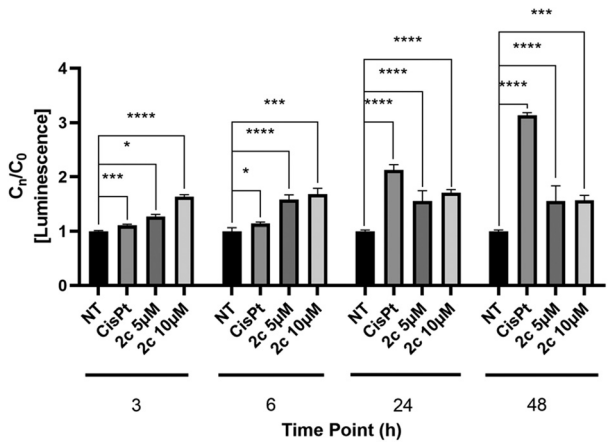

Fig. 7 Activation of caspases 3/7 as markers of apoptosis after 3, 6, 24 and 48 h of treatment with complex **2c**. OVCAR-5 cancer cells were treated with complex **2c** at concentrations of 5 μM and 10 μM. Results showed that the complex induced apoptosis in the OVCAR-5 cancer cell line. Positive control: cisplatin 10 μM. *p*-value was calculated *vs.* NT (untreated samples). (*p*-values: * ≤ 0.05, ** ≤ 0.01, *** ≤ 0.001, **** ≤ 0.0001.)

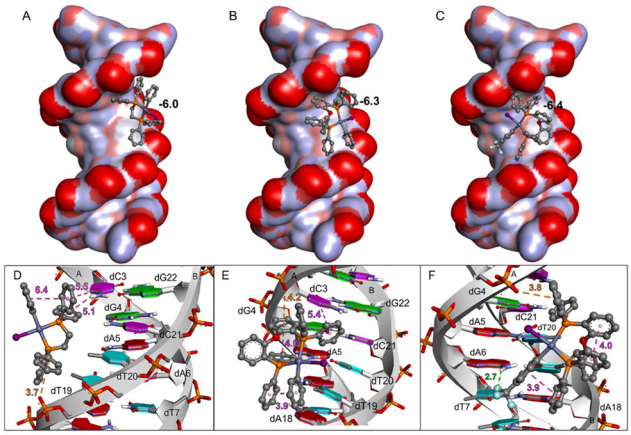

Fig. 8 DNA interactions with Pd(II) complexes (A) [PdI(Ph)(dppe)], (B) [PdI(Ph)(DPEphos)], and (C) [PdI(*p*-CF_3-Ph)(DPEphos)]. Close-up view of the binding pose and interactions between DNA (PDB ID 1BNA) and (D) [PdI(Ph)(dppe)], (E) [PdI(Ph)(DPEphos)], and (F) [PdI(*p*-CF_3-Ph)(DPEphos)]. At the top, DNA is represented by a surface model colored by atom charges, and the Pd(II) complexes are shown as ball-and-stick models. The predicted binding energies (Δ*G*) for [PdI(Ph)(dppe)] (A), [PdI(Ph)(DPEphos)] (B), and [PdI(*p*-CF_3-Ph)(DPEphos)] (C) were −6.0 kcal mol^{-1}, −6.3 kcal mol^{-1} and −6.4 kcal mol^{-1}, respectively. At the bottom, DNA is shown by the strands and rings in red, blue, pink, and green indicate deoxyadenosine (dA), deoxythymidine (dT), deoxycytidine (dC), and deoxyguanosine (dG) residues, respectively. Hydrophobic (π–π), H-bond, and electrostatic (anion–π) interactions are represented by purple, green, and orange dashed lines with their respective distances in Å.

were carried out. Three complexes have been considered: [PdI(Ph)(dppe)] (**2c**), [PdI(Ph)(DPEphos)] (**6c***), and [PdI(*p*-CF_3-Ph)(DPEphos)] (**6b**): the first and third show remarkable differences in biological activity and structurally exhibit a large difference in the diphosphine bite angle (86° *vs.* 102°, measured on the optimized molecular geometries). The second complex is a model that was considered because it has a close structural analogy to the third (both have a bite angle of 102°), but it lacks the CF_3 groups and so in principle the comparison allows us to separate the role of the bite angle from other relevant effects due to the ring substituents.

First, the *in silico* analysis demonstrates that the major groove region of DNA and the hydrophobic contacts with nucleotide residues are the main types of interactions for all three complexes (Fig. 8); this is in agreement with previous studies involving other Pd derivatives.[54]

Binding is thermodynamically favourable ($\Delta G \approx -6$ kcal mol^{-1}) in all cases and the energy values are very similar. Interestingly, the phenyl groups of [PdI(Ph)(dppe)] (**2c**) point directly into the groove, interacting mostly with deoxycytidine (dC) and deoxythymidine (dT) residues, while the Pd(II)–iodide moiety points outside this region. Conversely, the less reactive complexes ([PdI(Ph)(DPEphos)] (**6c***) and [PdI(*p*-CF_3-Ph)(DPEphos)] (**6b**)) present a different binding pose, due to steric hindrance caused by the Ph–O–Ph moiety, which imposes a larger bite angle. These molecules have intramolecular hydrophobic interactions, between the phenyl groups, and the Pd–I group is oriented parallel to the DNA. As shown in Fig. 9, [PdI(Ph)(dppe)] (**2c**) fits well into the major groove of DNA, with the hydrophobic region interacting with the DNA bases and the polar region (Pd–I moiety) being guided to the solvent-accessible area (water in the biological environment). On the other hand, [PdI(Ph)(DPEphos)] (**6c***) and [PdI(*p*-CF_3-Ph)(DPEphos)] (**6b**) show less favourable interactions with DNA. The Pd–I moiety of [PdI(Ph)(DPEphos)] (**6c***) binds in the hydrophobic region of the DNA groove, and the iodide ligand of [PdI(*p*-CF_3-Ph)(DPEphos)] (**6b**) interacts with the negative phosphate group of dG4, *i.e.*, the two negative regions are close (3.9 Å). In addition, the Pd complexes show Pd···O interactions (from 6 to 8 Å) involving the metal center and the

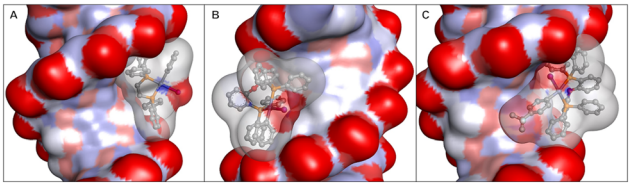

Fig. 9 Surface models of the binding pose of (A) [PdI(Ph)(dppe)], (B) [PdI(Ph)(DPEphos)], and (C) [PdI(*p*-CF_3-Ph)(DPEphos)] complexes with DNA. The surfaces are colored to indicate atom partial charges: red, blue, and grey indicate negative, positive, and neutral (or hydrophobic) regions.

oxygen atom from the phosphodiester group of the nucleotide residues. In fact, it has already been reported that Pd is able to interact both with the phosphate and the nitrogen bases of DNA.[55] In conclusion, complex [PdI(Ph)(dppe)] (**2c**) has the most favourable interactions with DNA, which may explain its remarkable biological activity.

Conclusions

In conclusion, a synthetic protocol for a wide range of Pd(II)–aryl complexes, bearing different diphosphine, halide and aryl ligands was developed, profitably modifying some procedures reported in the literature. In particular, the way to introduce chloride or bromide ligands into the palladium coordination sphere was original and involved the passage through an intermediate species equipped with a chelating thioquinoline ligand, from which it was possible to obtain the fast and complete substitution of the coordinated iodide with bromide or chloride by adding IBr or ICl, respectively.

A good portion of the prepared compounds are unpublished and for this reason their exhaustive characterization is provided and based on NMR, IR and HRMS analyses. Moreover, in some cases the solid-state structures were also defined by single crystal X-ray diffractometry.

In the case of complex [PdI(*p*-NO_2-Ph)(dppbz)] (**5a**), a kinetic and computational study allowed us to determine the kinetic constant and the mechanism for the formation of this complex.

This synthetic effort has provided us with a sufficient number of Pd(II)–aryl complexes to propose the first systematic study on the anticancer properties of this class of organopalladium compounds. These were tested on a selection of ovarian and breast cancer cell lines, showing IC_{50} values often comparable to, or even better than, cisplatin, which was taken as a reference metallodrug. Of particular significance is the fact that complexes **2c** and **2d** exhibited excellent cytotoxicity towards cancer cells and, at the same time, low activity on normal ones (human lung fibroblasts). These compounds contain a diphosphine ligand with a low bite angle (dppe) and electron-rich aryl fragments (phenyl or *para*-tolyl). As a result of these findings, [PdI(Ph)(dppe)] (**2c**) was chosen as a model for studying the mechanism of action of the complexes reported in this work. Immunofluorescence tests (cytochrome c and H2AX assays) seem to indicate DNA as the primary cellular target. Moreover, the activation of caspases 3 and 7 suggests that cell death occurs through an apoptotic pathway.

Remarkably, a detailed molecular docking study confirmed that the interaction between DNA and our Pd(II)–aryl complexes was stronger when diphosphine ligands with low bite angles were employed. In contrast, aryl and halide ligands appear to make a less significant contribution to the stability of the complex–DNA adduct and therefore to the antitumor activity of the synthesized complexes.

Finally, complex [PdI(Ph)(dppe)] (**2c**) showed promising cytotoxicity even on more complex and realistic biological models such as 3D organoids obtained from tumoral tissues of different real patients. Its activity is comparable to that of carboplatin, which is the reference compound for standard clinical therapy.

We believe that the high selectivity observed *in vitro* and the efficacy for the *ex vivo* models are good premises in view the of future clinical application of some compounds described in this paper. However, further studies aimed primarily at evaluating their *in vivo* efficacy are ongoing in our laboratories.

Experimental section

Solvents and reagents

All syntheses were carried out under an inert atmosphere using standard Schlenk techniques. The solvent CH_2Cl_2 was distilled over P_2O_5 and stored under a N_2 atmosphere. All other solvents and chemicals were commercial grade products and used as purchased. Complexes **1a–d**[21,22] and **7-I**[41] were synthesized according to published protocols.

NMR, UV-Vis and IR measurements

1D NMR and 2D NMR spectra were recorded on Bruker 300 or 400 Avance spectrometers. Chemical shift values (ppm) are given relative to TMS (^{1}H and ^{13}C), H_3PO_4 (^{31}P) and CCl_3F (^{19}F).

IR spectra were recorded on a PerkinElmer Spectrum One spectrophotometer. HRMS spectra were recorded on a Bruker Compact Q-TOF instrument. Mass spectra were recorded in positive mode.

Computational details

All calculations were performed by using DFT, as implemented in the ORCA 4.2 suite of *ab initio* quantum chemistry programs.[56] Geometry optimizations were performed with the B97M-D3BJ functional[57] by using the double-ζ-quality def2-SVP[58] basis set that included relativistic core potentials for Pd.

Solvent effects (dichloromethane, ε = 8.93) were included using CPCM. More accurate single-point energies were computed from the optimized geometries by using ωB97M-V[59] DFT and the triple-ζ-quality def2-TZVPP[58] basis set. Vibrational frequencies were computed at the B97M-D3BJ/def2-SVP level of theory to derive the Gibbs free energy.

The DNA blind docking studies were carried out using the AutoDock Vina 1.1.1 program,[60] using the B-DNA dodecamer crystallographic structure from the Protein Data Bank – PDB (ID 1BNA, sequence d(CGCGAATTCGCG)$_2$), according to previous studies.[61] The structures of the Pd complexes were obtained by full geometry optimizations using the BLYP potential[62] combined with a Slater triple zeta quality basis set with two polarization functions. The small core approximation was used and scalar relativistic effects were included using the ZORA approximation.[63] This level of theory, here denoted ZORA-BLYP/TZ2P, gave accurate results for compounds with heavy nuclei.[64] The DFT calculations were carried out using ADF2019.[65] Hirshfeld partial charges computed at the ZORA-BLYP/TZ2P level were used in the docking simulation and the DNA macromolecule was prepared using the Chimera 1.8 software.[66] Since AutoDock Vina does not recognize the Pd atom, it was replaced by Zn for docking simulations, but it retained all the properties of this metal center obtained from the quantum mechanical results. It was used with an exhaustiveness of 50, and the grid box was positioned in the center of the DNA structure (coordinates *xyz*: 14.75, 20.98, and 9.23; size: 50 × 50 × 50 Å). As a model of the binding pose, the ligand's conformers with the lowest predicted binding free energy (ΔG) were selected from the most populated cluster.

Synthesis of Pd–aryl complexes

[PdI(*p*-NO$_2$-Ph)(dppe)] (2a). To 0.0704 g (0.149 mmol) of [PdI(tmeda)(*p*-NO$_2$-Ph)] dissolved in 10 mL of anhydrous CH_2Cl_2, a solution of 0.0627 g (0.157 mmol) of dppe in 10 mL of anhydrous CH_2Cl_2 was added under an inert atmosphere (Ar). The resulting yellow solution was stirred for 15 min at room temperature. The solution was then concentrated under vacuum and the title complex was precipitated by the addition of diethyl ether and pentane, filtered through a sintered glass filter, and dried under vacuum. 0.0982 g (yield 87%) of complex **2a** was obtained as a yellow powder.

^{1}H NMR (300 MHz, $CDCl_3$, T = 298 K, ppm) δ: 2.18–2.51 (m, 4H, PCH_2), 7.27–7.56 (m, 20H, aryl–H), 7.84–7.91 (m, 4H, aryl–H).

^{13}C{^{1}H} NMR (75 MHz, $CDCl_3$, T = 298 K, ppm) δ: 25.2 (CH_2, dd, J_{C-P} = 25.9 Hz, 13.2 Hz, PCH_2), 29.7 (CH_2, dd, J_{C-P} = 30.0 Hz, 20.8 Hz, PCH_2), 120.3, 120.4, 128.3, 128.9, 129.1, 129.1, 129.2, 129.3, 130.4, 130.9, 131.3, 131.4, 131.9, 131.9, 133.0, 133.2, 133.8, 133.9, 137.7, 137.8, 137.8, 137.8, 144.7, 172.0, 173.8.

^{31}P{^{1}H} NMR (121 MHz, $CDCl_3$, T = 298 K, ppm) δ: 37.5 (d, J_{P-P} = 26.1 Hz), 51.0 (d, J_{P-P} = 26.1 Hz).

IR (KBr pellet, cm^{-1}): ν_{NO_2} = 1335, 1497.

HRMS calcd for $[C_{32}H_{28}INNaO_2P_2Pd]^+$: 775.9579; found: 775.9577.

[PdI(*p*-CF$_3$-Ph)(dppe)] (2b). Complex **2b** was obtained in the same manner as complex **2a** by employing 0.0461 g (0.0932 mmol) of [PdI(tmeda)(*p*-CF$_3$-Ph)] dissolved in 10 mL of anhydrous CH_2Cl_2 and 0.0413 g (0.104 mmol) of dppe in 10 mL of anhydrous CH_2Cl_2. Complex **2b** was precipitated by the addition of diethyl ether. 0.0591 g (yield 82%) of complex **2b** was obtained as a yellow solid.

^{1}H NMR (400 MHz, $CDCl_3$, T = 298 K, ppm) δ: 2.17–2.46 (m, 4H, PCH_2), 6.93 (*pseudo* d, 2H, J_{H-H} = 7.0 Hz, aryl–H), 7.20 (*pseudo* t, 2H, J_{H-H} = 7.9 Hz, aryl–H), 7.32–7.37 (m, 8H, aryl–H), 7.45–7.52 (m, 8H, aryl–H), 7.89 (*pseudo* t, 4H, J_{H-H} = 8.2 Hz, aryl–H).

^{31}P{^{1}H} NMR (162 MHz, $CDCl_3$, T = 298 K, ppm) δ: 35.5 (d, J_{P-P} = 27.2 Hz), 50.2 (d, J_{P-P} = 27.2 Hz).

^{19}F{^{1}H} NMR (377 MHz, $CDCl_3$, T = 298 K, ppm) δ: −61.9.

Data are in agreement with the reported values.[38]

[PdI(Ph)(dppe)] (2c). Complex **2c** was obtained in the same manner as complex **2a** by employing 0.0506 g (0.119 mmol) of [PdI(tmeda)(Ph)] dissolved in 10 mL of anhydrous CH_2Cl_2 and 0.0525 g (0.132 mmol) of dppe in 10 mL of anhydrous CH_2Cl_2. Complex **2c** was precipitated by the addition of diethyl ether. 0.0826 g (yield 98%) of complex **2c** was obtained as a yellow solid.

^{1}H NMR (300 MHz, $CDCl_3$, T = 298 K, ppm) δ: 2.13–2.46 (m, 4H, PCH_2), 6.62–6.75 (m, 3H, aryl–H), 7.09 (*pseudo* t, 2H, J_{H-H} = 7.8 Hz, aryl–H), 7.29–7.48 (m, 16H, aryl–H), 7.87–7.93 (m, 4H, aryl–H).

^{31}P{^{1}H} NMR (121 MHz, $CDCl_3$, T = 298 K, ppm) δ: 34.0 (d, J_{P-P} = 27.9 Hz), 48.9 (d, J_{P-P} = 27.9 Hz).

Data are in agreement with the reported values.[40]

[PdI(*p*-CH$_3$-Ph)(dppe)] (2d). Complex **2d** was obtained in the same manner as complex **2a** by employing 0.0598 g (0.136 mmol) of [PdI(tmeda)(*p*-CH$_3$-Ph)] dissolved in 10 mL of anhydrous CH_2Cl_2 and 0.0601 g (0.151 mmol) of dppe in 10 mL of anhydrous CH_2Cl_2. Complex **2d** was precipitated by the addition of diethyl ether. 0.0800 g (yield 82%) of complex **2d** was obtained as a yellow solid.

^{1}H NMR (300 MHz, CDCl,^{3} T = 298 K, ppm) δ: 2.10 (s, 3H, CH_3), 2.13–2.45 (m, 4H, PCH_2), 6.57–6.61 (m, 2H, aryl–H), 6.90–6.96 (m, 2H, aryl–H), 7.28–7.48 (m, 16H, aryl–H), 7.86–7.93 (m, 4H, aryl–H).

^{31}P{^{1}H} NMR (121 MHz, $CDCl_3$, T = 298 K, ppm) δ: 33.9 (d, J_{P-P} = 27.6 Hz), 48.7 (d, J_{P-P} = 27.6 Hz).

Data are in agreement with the reported values.[40]

[PdI(*p*-NO$_2$-Ph)(dppp)] (3a). Complex **3a** was obtained in the same manner as complex **2a** by employing 0.0714 g (0.151 mmol) of [PdI(tmeda)(*p*-NO$_2$-Ph)] dissolved in 10 mL of anhydrous CH_2Cl_2 and 0.0692 g (0.168 mmol) of dppp in 10 mL of anhydrous CH_2Cl_2. Complex **3a** was precipitated by the addition of diethyl ether. 0.1061 g (yield 91%) of complex **3a** was obtained as a yellow solid.

^{1}H NMR (300 MHz, $CDCl_3$, T = 298 K, ppm) δ: 1.83–2.04 (m, 2H, CH_2), 2.40–2.47 (m, 2H, PCH_2), 2.53–2.60 (m, 2H, PCH_2), 7.12–7.25 (7H, aryl–H), 7.27–7.46 (13H, aryl–H), 7.75–7.80 (4H, aryl–H).

^{13}C{^{1}H} NMR (75 MHz, $CDCl_3$, T = 298 K, ppm) δ: 19.1 (CH_2, d, J_{C-P} = 2.3 Hz, CH_2), 26.7 (CH_2, dd, J_{C-P} = 21.1 Hz, 3.8 Hz, PCH_2), 28.0 (CH_2, dd, J_{C-P} = 24.9 Hz, 7.3 Hz, PCH_2), 120.2, 120.4, 128.5, 128.7, 128.8, 129.8, 130.4, 130.7, 131.0, 132.0, 132.5, 133.0, 133.2, 133.7, 133.8, 137.1, 144.1, 171.8, 173.5.

^{31}P{^{1}H} NMR (121 MHz, CDCl3, T = 298 K, ppm) δ: −9.9 (d, J_{P-P} = 52.6 Hz), 9.7 (d, J_{P-P} = 52.6 Hz).

IR (KBr pellet, cm^{-1}): ν_{NO_2} = 1334, 1495.

Data are in agreement with the reported values.[37]

[PdI(*p*-CF_3-Ph)(dppp)] (3b). Complex **3b** was obtained in the same manner as complex **2a** by employing 0.0715 g (0.145 mmol) of [PdI(tmeda)(*p*-CF_3-Ph)] dissolved in 10 mL of anhydrous CH_2Cl_2 and 0.0658 g (0.160 mmol) of dppp in 10 mL of anhydrous CH_2Cl_2. Complex **3b** was precipitated by the addition of diethyl ether. 0.0958 g (yield 84%) of complex **3a** was obtained as a yellow solid.

^{1}H NMR (300 MHz, $CDCl_3$, T = 298 K, ppm) δ: 1.80–2.02 (m, 2H, CH_2), 2.39–2.46 (m, 2H, PCH_2), 2.52–2.59 (m, 2H, PCH_2), 6.73–6.76 (m, 2H, aryl–H), 7.02–7.08 (m, 2H, aryl–H), 7.11–7.17 (m, 4H, aryl–H), 7.22–7.35 (m, 7H, aryl–H), 7.42–7.48 (m, 5H, aryl–H), 7.76–7.83 (m, 4H, aryl–H).

^{13}C{^{1}H} NMR (75 MHz, $CDCl_3$, T = 298 K, ppm, *selected peaks*) δ: 19.2 (CH_2, d, J_{C-P} = 2.9 Hz, CH_2), 26.9 (CH_2, dd, J_{C-P} = 19.9 Hz, 4.2 Hz, PCH_2), 28.2 (CH_2, dd, J_{C-P} = 25.9 Hz, 7.1 Hz, PCH_2), 124.1 (C, q, J_{C-F} = 31.3 Hz, *p*-aryl–C), 125.1 (C, q, J_{C-F} = 271.3 Hz, CF_3), 122.8, 122.9, 122.9, 123.0, 128.4, 128.6, 128.6, 128.7, 130.2, 130.5, 130.5, 130.7, 130.7, 130.9, 132.3, 132.8, 133.0, 133.2, 133.7, 133.9, 136.9, 136.9, 136.9, 162.0, 163.8.

^{31}P{^{1}H} NMR (121 MHz, $CDCl_3$, T = 298 K, ppm) δ: −10.3 (d, J_{P-P} = 53.3 Hz), 10.3 (d, J_{P-P} = 53.3 Hz).

^{19}F{^{1}H} NMR (377 MHz, $CDCl_3$, T = 298 K, ppm) δ: −61.9.

Data are in agreement with the reported values.[37]

[PdI(*p*-NO_2-Ph)(dppf)] (4a). Complex **4a** was obtained in the same manner as complex **2a** by employing 0.0703 g (0.149 mmol) of [PdI(tmeda)(*p*-NO_2-Ph)] dissolved in 10 mL of anhydrous CH_2Cl_2 and 0.0912 g (0.165 mmol) of dppf in 10 mL of anhydrous CH_2Cl_2. Complex **4a** was precipitated by the addition of diethyl ether. 0.1320 g (yield 97%) of complex **4a** was obtained as a yellow solid.

^{1}H NMR (300 MHz, $CDCl_3$, T = 298 K, ppm) δ: 3.67 (q, 2H, J_{H-H} = 1.8 Hz, Fc–H), 4.17 (t, 2H, J_{H-H} = 1.9 Hz, Fc–H), 4.53 (t, 2H, J_{H-H} = 1.9 Hz, Fc–H), 4.70 (q, 2H, J_{H-H} = 2.1 Hz, Fc–H), 7.10–7.16 (m, 4H, aryl–H), 7.18–7.24 (m, 2H, aryl–H), 7.31–7.40 (m, 8H, aryl–H), 7.49–7.52 (m, 6H, aryl–H), 7.98–8.05 (m, 4H, aryl–H).

^{13}C{^{1}H} NMR (75 MHz, $CDCl_3$, T = 298 K, ppm, selected peaks) δ: 72.4 (CH, d, J_{C-P} = 5.0 Hz, Fc-CH), 73.8 (CH, d, J_{C-P} = 7.4 Hz, Fc-CH), 74.6 (CH, d, J_{C-P} = 8.2 Hz, Fc-CH), 76.2 (CH, d, J_{C-P} = 12.0 Hz, Fc-CH), 120.5, 120.7, 128.2, 128.3, 128.4, 128.4, 130.7, 130.7, 130.9, 130.9, 132.1, 132.8, 133.0, 133.5, 133.9, 134.1, 135.6, 135.7, 137.1, 144.2.

^{31}P{^{1}H} NMR (121 MHz, $CDCl_3$, T = 298 K, ppm) δ: 9.3 (d, J_{P-P} = 32.0 Hz), 26.2 (d, J_{P-P} = 32.0 Hz).

IR (KBr pellet, cm^{-1}): ν_{NO_2} = 1337, 1502.

[PdI(*p*-CF_3-Ph)(dppf)] (4b). Complex **4b** was obtained in the same manner as complex **2a** by employing 0.0459 g (0.0927 mmol) of [PdI(tmeda)(*p*-CF_3-Ph)] dissolved in 10 mL of anhydrous CH_2Cl_2 and 0.0580 g (0.105 mmol) of dppf in 10 mL of anhydrous CH_2Cl_2. Complex **4b** was precipitated by the addition of diethyl ether. 0.0785 g (yield 91%) of complex **4b** was obtained as a yellow solid.

^{1}H NMR (300 MHz, $CDCl_3$, T = 298 K, ppm) δ: 3.69 (q, 2H, J_{H-H} = 1.8 Hz, Fc–H), 4.15 (t, 2H, J_{H-H} = 1.9 Hz, Fc–H), 4.50 (t, 2H, J_{H-H} = 1.9 Hz, Fc–H), 4.67 (q, 2H, J_{H-H} = 2.0 Hz, Fc–H), 6.72–6.76 (m, 2H, aryl–H), 7.06–7.16 (m, 6H, aryl–H), 7.30–7.38 (m, 6H, aryl–H), 7.47–7.52 (m, 6H, aryl–H), 7.99–8.06 (m, 4H, aryl–H).

^{31}P{^{1}H} NMR (121 MHz, $CDCl_3$, T = 298 K, ppm) δ: 8.7 (d, J_{P-P} = 33.5 Hz), 26.5 (d, J_{P-P} = 33.5 Hz).

^{19}F{^{1}H} NMR (377 MHz, $CDCl_3$, T = 298 K, ppm) δ: −61.9.

Data are in agreement with the reported values.[21]

[PdI(Ph)(dppf)] (4c). Complex **4c** was obtained in the same manner as complex **2a** by employing 0.0511 g (0.120 mmol) of [PdI(tmeda)(Ph)] dissolved in 10 mL of anhydrous CH_2Cl_2 and 0.0742 g (0.134 mmol) of dppf in 10 mL of anhydrous CH_2Cl_2. Complex **4c** was precipitated by the addition of diethyl ether. 0.0960 g (yield 93%) of complex **4c** was obtained as a yellow solid.

^{1}H NMR (300 MHz, $CDCl_3$, T = 298 K, ppm) δ: 3.70 (q, 2H, J_{H-H} = 1.8 Hz, Fc–H), 4.13 (t, 2H, J_{H-H} = 1.9 Hz, Fc–H), 4.47 (t, 2H, J_{H-H} = 1.9 Hz, Fc–H), 4.64 (q, 2H, J_{H-H} = 2.1 Hz, Fc–H), 6.40–6.45 (m, 1H, aryl–H), 6.51–6.57 (m, 2H, aryl–H), 6.90–6.97 (m, 2H, aryl–H), 7.09–7.15 (m, 4H, aryl–H), 7.28–7.40 (m, 6H, aryl–H), 7.45–7.50 (m, 6H, aryl–H), 8.00–8.07 (m, 4H, aryl–H).

^{31}P{^{1}H} NMR (121 MHz, $CDCl_3$, T = 298 K, ppm) δ: 8.0 (d, J_{P-P} = 34.5 Hz), 26.4 (d, J_{P-P} = 34.5 Hz).

Data are in agreement with the reported values.[40]

[PdI(*p*-CH_3-Ph)(dppf)] (4d). Complex **4d** was obtained in the same manner as complex **2a** by employing 0.0704 g (0.160 mmol) of [PdI(tmeda)(*p*-CH_3-Ph)] dissolved in 10 mL of anhydrous CH_2Cl_2 and 0.0981 g (0.177 mmol) of dppf in 10 mL of anhydrous CH_2Cl_2. Complex **4d** was precipitated by the addition of diethyl ether. 0.1386 g (yield 99%) of complex **4d** was obtained as a yellow solid.

^{1}H NMR (400 MHz, $CDCl_3$, T = 298 K, ppm) δ: 2.01 (s, 3H, CH_3), 3.72 (q, 2H, J_{H-H} = 1.8 Hz, Fc–H), 4.12 (t, 2H, J_{H-H} = 1.9 Hz, Fc–H), 4.45 (t, 2H, J_{H-H} = 1.9 Hz, Fc–H), 4.63 (q, 2H, J_{H-H} = 2.1 Hz, Fc–H), 6.39 (pseudo d, 2H, J_{H-H} = 7.6 Hz, aryl–H), 6.78 (pseudo td, 2H, J_{H-H} = 7.9 Hz, 2.4 Hz, aryl–H), 7.12 (pseudo td, 4H, J_{H-H} = 7.8 Hz, 2.3 Hz, aryl–H), 7.29–7.39 (m, 7H, aryl–H), 7.46–7.48 (m, 5H, aryl–H), 8.01–8.06 (m, 4H, aryl–H).

[PdI(*p*-NO_2-Ph)(dppbz)] (5a). To 0.0711 g (0.151 mmol) of [PdI(tmeda)(*p*-NO_2-Ph)] dissolved in 10 mL of anhydrous CH_2Cl_2, a solution of 0.0751 g (0.168 mmol) of dppbz in 10 mL of anhydrous CH_2Cl_2 was added under an inert atmosphere (Ar). The resulting yellow solution was stirred for 1 hour at room temperature. The solution was then concentrated under vacuum and the title complex was precipitated by the addition of diethyl ether, filtered through a sintered glass filter, and dried under vacuum. 0.1020 g (yield 84%) of complex **5a** was obtained as a yellow powder.

^{1}H NMR (300 MHz, $CDCl_3$, T = 298 K, ppm) δ: 7.23–7.73 (28H, aryl–H).

^{13}C{^{1}H} NMR (75 MHz, $CDCl_3$, T = 298 K, ppm, *selected peaks*) δ: 120.1, 120.3, 128.6, 128.9, 129.0, 129.0, 129.1, 129.3, 130.9, 131.2, 131.2, 131.4, 131.6, 131.6, 132.0, 132.2, 132.3, 132.6, 133.2, 133.4, 133.6, 133.8, 134.1, 134.3, 134.6, 134.8, 137.9, 137.9, 138.0, 144.9.

$^{31}P\{^1H\}$ NMR (121 MHz, $CDCl_3$, T = 298 K, ppm) δ: 45.1 (d, J_{P-P} = 26.4 Hz), 51.2 (d, J_{P-P} = 26.4 Hz).

IR (KBr pellet, cm^{-1}): ν_{NO_2} = 1339, 1500.

HRMS calcd for $[C_{36}H_{28}INNaO_2P_2Pd]^+$: 823.9581; found: 823.9584.

[PdI(*p*-CF_3-Ph)(dppbz)] (5b). Complex **5b** was obtained in the same manner as complex **5a** by employing 0.0710 g (0.144 mmol) of [PdI(tmeda)(*p*-CF_3-Ph)] dissolved in 10 mL of anhydrous CH_2Cl_2 and 0.0706 g (0.158 mmol) of dppbz in 10 mL of anhydrous CH_2Cl_2. Complex **5b** was precipitated by the addition of diethyl ether. 0.0894 g (yield 76%) of complex **5b** was obtained as a light pink solid.

^1H NMR (400 MHz, $CDCl_3$, T = 298 K, ppm) δ: 6.93–7.72 (28H, aryl–H).

$^{13}C\{^1H\}$ NMR (75 MHz, $CDCl_3$, T = 298 K, ppm, selected peaks) δ: 122.7, 122.8, 122.8, 122.9, 123.5, 124.7, 125.2, 126.5, 127.1, 127.2, 128.8, 128.8, 129.0, 129.7, 131.0, 131.0, 131.2, 131.3, 131.3, 131.7, 132.1, 132.2, 132.4, 132.4, 133.3, 133.4, 133.6, 133.9, 134.1, 134.3, 134.6, 134.8, 137.5, 137.6, 137.6, 162.5, 164.3.

$^{31}P\{^1H\}$ NMR (162 MHz, $CDCl_3$, T = 298 K, ppm) δ: 43.8 (d, J_{P-P} = 27.4 Hz), 51.1 (d, J_{P-P} = 27.4 Hz).

$^{19}F\{^1H\}$ NMR (377 MHz, $CDCl_3$, T = 298 K, ppm) δ: −61.8.

HRMS calcd for $[C_{37}H_{28}F_3INaP_2Pd]^+$: 846.9604; found: 846.9619.

[PdI(*p*-NO_2-Ph)(DPEphos)] (6a). Complex **6a** was obtained in the same manner as complex **2a** by employing 0.0706 g (0.150 mmol) of [PdI(tmeda)(*p*-NO_2-Ph)] dissolved in 10 mL of anhydrous CH_2Cl_2 and 0.0891 g (0.165 mmol) of DPEphos in 10 mL of anhydrous CH_2Cl_2. 0.1298 g (yield 97%) of complex **6a** was obtained as a yellow solid.

^1H NMR (300 MHz, $CDCl_3$, T = 233 K, ppm) δ: 6.54–7.89 (m, 32H, aryl–H).

$^{13}C\{^1H\}$ NMR (75 MHz, $CDCl_3$, T = 298 K, ppm, selected peaks) δ: 120.2, 123.4, 123.9, 128.0, 128.1, 130.2, 133.9, 135.6, 137.8, 144.1, 158.5, 158.6.

$^{31}P\{^1H\}$ NMR (121 MHz, $CDCl_3$, T = 233 K, ppm) δ: 5.2 (d, J_{P-P} = 33.0 Hz), 9.7 (d, J_{P-P} = 33.0 Hz).

IR (KBr pellet, cm^{-1}): ν_{NO_2} = 1336, 1499.

[PdI(*p*-CF_3-Ph)(DPEphos)] (6b). Complex **6b** was obtained in the same manner as complex **2a** by employing 0.0748 g (0.151 mmol) of [PdI(tmeda)(*p*-CF_3-Ph)] dissolved in 10 mL of anhydrous CH_2Cl_2 and 0.0900 g (0.167 mmol) of DPEphos in 10 mL of anhydrous CH_2Cl_2. Complex **6b** was precipitated by the addition of diethyl ether. 0.1363 g (yield 98%) of complex **6b** was obtained as a yellow solid.

^1H NMR (300 MHz, CD_2Cl_2, T = 233 K, ppm) δ: 6.41–7.91 (m, 32H, aryl–H).

$^{13}C\{^1H\}$ NMR (75 MHz, $CDCl_3$, T = 233 K, ppm) δ: 117.7, 117.8, 123.0, 123.1, 123.4, 123.5, 123.5, 123.8, 123.8, 123.9, 124.0, 124.0, 124.1, 125.2, 125.3, 126.7, 127.7, 127.8, 128.0, 128.1, 128.2, 129.8, 130.0, 131.4, 132.6, 133.5, 135.4, 158.1, 158.2, 158.3, 158.3.

$^{31}P\{^1H\}$ NMR (121 MHz, CD_2Cl_2, T = 233 K, ppm) δ: 4.3 (d, J_{P-P} = 34.0 Hz), 10.4 (d, J_{P-P} = 34.0 Hz).

$^{19}F\{1H\}$ NMR (377 MHz, CD_2Cl_2, T = 298 K, ppm) δ: −61.9.

IR (KBr pellet, cm^{-1}): ν_{NO_2} = 1336, 1499.

HRMS calcd for $[C_{43}H_{32}F_3INaOP_2Pd]^+$: 938.9868; found: 938.9887.

[PdBr(*p*-NO_2-Ph)(TtBQ)] (7-Br). To 0.0794 g (0.139 mmol) of [PdI(*p*-NO_2-Ph)(TtBQ)] dissolved in 10 mL anhydrous CH_2Cl_2, a solution of 0.0344 g (0.166 mmol) of iodine monobromide in 6 mL of anhydrous CH_2Cl_2 was slowly added dropwise under an inert atmosphere. The resulting dark red solution was stirred at r.t. for 10 minutes and then filtered through an MF-Millipore™ membrane. The solution was then concentrated under vacuum and the title complex was precipitated by the addition of diethyl ether, filtered through a sintered glass filter, and dried under vacuum. 0.0724 g (yield 99%) of complex **7-Br** was obtained as a light brown powder.

^1H NMR (300 MHz, $CDCl_3$, T = 298 K, ppm) δ: 1.23 (s, 9H, *t*-Bu), 7.66–7.79 (m, 4H, H^3, H^6, Ph), 7.85–7.90 (m, 2H, Ph), 8.08 (dd, 1H, J_{H-H} = 7.3 Hz, 1.3 Hz, H^7), 8.10 (dd, 1H, J_{H-H} = 8.0 Hz, 1.3 Hz, H^5), 8.45 (dd, 1H, J_{H-H} = 8.3 Hz, 1.6 Hz, H^4), 9.95 (*pseudo* d, 1H, J_{H-H} = 4.9 Hz, H^2).

$^{13}C\{^1H\}$ NMR (75 MHz, $CDCl_3$, T = 298 K, ppm) δ: 30.7 (CH_3, *t*-Bu), 59.5 (C, *t*-Bu), 120.7 (CH, Ph), 123.6 (CH, C^3), 127.4 (CH, C^6), 129.6 (C, C^{4a}), 130.3 (C, C^8), 131.8 (CH, C^5), 137.7 (CH, C^7), 138.9 (CH, Ph), 139.1 (CH, C^4), 145.7 (C, Ph), 148.8 (C, C^{8a}), 152.2 (C, Ph), 155.1 (CH, C^2).

IR (KBr pellet, cm^{-1}): ν_{NO_2} = 1338, 1500.

[PdCl(*p*-NO_2-Ph)(TtBQ)] (7-Cl). To 0.0762 g (0.133 mmol) of [PdI(*p*-NO_2-Ph)(TtBQ)] dissolved in 10 mL anhydrous CH_2Cl_2, a solution of 0.0216 g (0.133 mmol) of iodine monochloride in 6 mL of anhydrous CH_2Cl_2 was slowly added dropwise under an inert atmosphere. The resulting purple solution was stirred at r.t. for 10 minutes. The solution was then concentrated under vacuum and the title complex was precipitated by the addition of diethyl ether, filtered through a sintered glass filter, and dried under vacuum. 0.0531 g (yield 83%) of complex **7-Cl** was obtained as a beige powder.

^1H NMR (300 MHz, $CDCl_3$, T = 298 K, ppm) δ: 1.23 (s, 9H, *t*-Bu), 7.68–7.80 (m, 4H, H^3, H^6, Ph), 7.86–7.91 (m, 2H, Ph), 8.08 (dd, 1H, J_{H-H} = 7.5 Hz, 1.3 Hz, H^7), 8.11 (dd, 1H, J_{H-H} = 8.4 Hz, 1.3 Hz, H^5), 8.46 (dd, 1H, J_{H-H} = 8.4 Hz, 1.6 Hz, H^4), 9.78 (dd, 1H, J_{H-H} = 4.9 Hz, 1.6 Hz, H^2).

$^{13}C\{^1H\}$ NMR (75 MHz, $CDCl_3$, T = 298 K, ppm) δ: 30.6 (CH_3, *t*-Bu), 59.4 (C, *t*-Bu), 120.8 (CH, Ph), 123.4 (CH, C^3), 127.4 (CH, C^6), 129.5 (C, C^{4a}), 130.2 (C, C^8), 131.8 (CH, C^5), 137.5 (CH, C^7), 138.2 (CH, Ph), 139.2 (CH, C^4), 145.7 (C, Ph), 148.7 (C, C^{8a}), 153.5 (CH, C^2), 153.8 (C, Ph).

IR (KBr pellet, cm^{-1}): ν_{NO_2} = 1337, 1499.

[PdCl(*p*-NO_2-Ph)(dppf)] (4a-Cl). To 0.0273 g (0.0567 mmol) of [PdCl(*p*-NO_2-Ph)(TtBQ)] dissolved in 13 mL of anhydrous CH_2Cl_2, 0.0353 g (0.0637 mmol) of dppf were added under an inert atmosphere (Ar). The resulting yellow solution was stirred for 15 min at room temperature. The solution was then concentrated under vacuum and the title complex was precipitated by the addition of diethyl ether, filtered through a sintered glass filter, and dried under vacuum. 0.0462 g (yield 99%) of complex **4a-Cl** was obtained as a yellow powder.

^{1}H NMR (300 MHz, $CDCl_3$, T = 298 K, ppm) δ: 3.58 (q, 2H, J_{H-H} = 1.9 Hz, Fc–H), 4.19 (t, 2H, J_{H-H} = 1.9 Hz, Fc–H), 4.54 (t, 2H, J_{H-H} = 1.9 Hz, Fc–H), 4.73 (q, 2H, J_{H-H} = 2.1 Hz, Fc–H), 7.09–7.26 (m, 6H, aryl–H), 7.30–7.51 (m, 14H, aryl–H), 8.02–8.08 (m, 4H, aryl–H).

^{13}C{^{1}H} NMR (75 MHz, $CDCl_3$, T = 298 K, ppm, selected peaks) δ: 72.5 (CH, d, J_{C-P} = 5.0 Hz, Fc–H), 74.0 (CH, d, J_{C-P} = 7.8 Hz, Fc–H), 74.7 (CH, d, J_{C-P} = 8.1 Hz, Fc–H), 76.4 (CH, d, J_{C-P} = 12.3 Hz, Fc–H), 121.1, 121.2, 128.2, 128.4, 128.5, 128.6, 130.6, 130.7, 131.0, 131.0, 132.1, 132.2, 132.6, 132.9, 134.0, 134.1, 135.1, 135.2, 135.2, 135.4, 144.3.

^{31}P{^{1}H} NMR (121 MHz, $CDCl_3$, T = 298 K, ppm) δ: 11.3 (d, J_{P-P} = 31.0 Hz), 31.5 (d, J_{P-P} = 31.0 Hz).

IR (KBr pellet, cm^{-1}): ν_{NO_2} = 1339, 1504.

[PdBr(*p*-NO_2-Ph)(dppf)] (4a-Br). Complex **4a-Br** was obtained in the same manner as complex **4a-Cl** by employing 0.0528 g (0.100 mmol) of [PdBr(*p*-NO_2-Ph)(TtBQ)] dissolved in 20 mL of anhydrous CH_2Cl_2 and 0.0619 g (0.112 mmol) of dppf. 0.0797 g (yield 92%) of complex **4a-Br** was obtained as a light orange solid.

^{1}H NMR (300 MHz, $CDCl_3$, T = 298 K, ppm) δ: 3.62 (q, 2H, J_{H-H} = 1.8 Hz, Fc–H), 4.18 (t, 2H, J_{H-H} = 1.8 Hz, Fc–H), 4.54 (t, 2H, J_{H-H} = 1.9 Hz, Fc–H), 4.72 (q, 2H, J_{H-H} = 2.1 Hz, Fc–H), 7.10–7.24 (m, 6H, aryl–H), 7.30–7.42 (m, 8H, aryl–H), 7.47–7.52 (m, 6H, aryl–H), 8.00–8.07 (m, 4H, aryl–H).

^{13}C{^{1}H} NMR (75 MHz, $CDCl_3$, T = 298 K, ppm, selected peaks) δ: 72.5 (CH, d, J_{C-P} = 4.9 Hz, Fc–H), 73.9 (CH, d, J_{C-P} = 7.6 Hz, Fc–H), 74.6 (CH, d, J_{C-P} = 8.2 Hz, Fc–H), 76.3 (CH, d, J_{C-P} = 12.3 Hz, Fc–H), 121.0, 121.1, 128.2, 128.4, 128.5, 130.6, 130.7, 131.0, 131.0, 132.1, 132.4, 132.8, 132.9, 134.0, 134.1, 135.3, 135.5, 135.6, 135.7, 144.2.

^{31}P{^{1}H} NMR (121 MHz, $CDCl_3$, T = 298 K, ppm) δ: 10.4 (d, J_{P-P} = 31.2 Hz), 30.3 (d, J_{P-P} = 31.2 Hz).

IR (KBr pellet, cm^{-1}): ν_{NO_2} = 1338, 1503.

Cell viability assay

Four cancer cells lines (A2780, A2780*cis*, OVCAR-5, MDA-MB-231) and one non-tumoral cell type (MRC-5) were employed and grown in accordance with the supplier's instructions and maintained at 37 °C under a humidified atmosphere of 5% of CO_2. A defined number of cells (A2780 1000 cells per well (cpw), A2780*cis* 2500 cpw, OVCAR-5 2000 cpw, MDA-MB-231 1000 cpw and MRC-5 8000 cpw) were seeded in 96 wells and after 24 h treated with six different concentrations of Pd(II) complexes (0.001, 0.01, 0.1, 1, 10, 100 μM). 96 h after treatment, the cell viability was measured with a CellTiter glow assay (Promega, Madison, WI, USA) with BioTek Synergy H1. IC_{50} values were calculated from logistic dose–response curves. Averages were obtained from experiments carried out in triplicate and error bars are standard deviations.

Organoid cultures

Specimens underwent complete anonymization prior to the derivation of organoids. Nonetheless, participants provided informed consent for research utilization of the samples, facilitated through the biobank at the National Cancer Institute (CRO) in Aviano. Primary tumor samples were subjected to a pre-processing incubation in Dulbecco's modified Eagle's medium/nutrient mixture F-12 ham supplemented with a cocktail of antimicrobial agents (levofloxacin 100 μg mL^{-1}, vancotex 25 μg mL^{-1}, ciproxin 5 μg mL^{-1}, gentamicin 200 μg mL^{-1}, and fungizone 5 μg mL^{-1}) for 30 minutes. Subsequently, tissues were meticulously minced to 0.5–1 mm^3 fragments, treated with a 4 mg mL^{-1} solution of collagenase IV (Gibco, Massachusetts, USA), and incubated at 37 °C, avoiding exceeding 45-minute enzyme exposure. Mechanical disaggregation was achieved *via* pipetting. Following centrifugation at 1000 rpm for 10 minutes, the cellular aggregates were resuspended in Cultrex RGF BME, Type 2 (Bio-techne, Minnesota, USA), and seeded in 24-well culture plates for maintenance. Once the Cultrex matrix solidified, each well received 500 μL of organoid medium, refreshed tri-weekly as delineated by Kopper *et al.*[46] The organoids were then maintained in a controlled environment at 37 °C under a 5% CO_2 atmosphere.

Organoids' half-maximal inhibitory concentration (IC_{50})

Clusters of PDOs were mixed in an appropriate volume of Cultrex RGF BME, Type 2 (Bio-techne, Minnesota, USA) and 2 μL of this mixture were seeded in 96-well plates and treated with six different concentrations of carboplatin (0.032, 0.16, 0.8, 4, 20, 100 μM) and compound **2c** (0.016, 0.08, 0.4, 2, 10, 50 μM) in four replicates. After 96 h, cell viability was measured using CellTiter-Glo 3D (Promega, Madison, WI, USA) with BioTek Synergy H1. Logistic dose–response curves were used to calculate IC_{50} using GraphPad Prism (La Jolla, CA, US).

DNA damage assay

OVCAR-5 cells were seeded (20 000 cells per well) on chamber slides. After overnight culture at 37 °C and 5% CO_2, cells were treated with different concentrations of compound **2c** (5 and 10/25 μM) or cisplatin (10 μM) for 6, 24, and 48 h. Cells were fixed in 4% paraformaldehyde/PBS (20 min, RT), permeabilized with 0.3% Triton X-100/PBS (15 min, RT) and blocked in 8% BSA/PBS (1 h, RT). Cells were incubated with rabbit monoclonal anti-Ser^{139}γH2A.X antibody (Cell Signaling Cat. #9718 Burlington, MA, USA, 1 : 100 dilution in 1% BSA/PBS, at 4 °C, overnight). Samples incubated with Ser^{139}γH2A.X were labeled with secondary antibody (Goat anti-Rabbit Alexa Fluor™ 488, 1 : 1000 dilution, RT, 1 h) obtained from Cell Signaling Technology (Cat. #A32731; Danvers, MA, US). To visualize nuclei, cells were stained with 1 mg mL^{-1} DAPI (in PBS, RT, 1 min). Cells were washed three times with PBS after all incubations. All the chamber slides were mounted with fluorSave™ reagent (Cat. #345789; Millipore: Burlington, MA, USA).

Cells were examined with a NIKON Eclipse TI2 (equipped with X-Light V2 L-FOV spinning disk and lumencore lamp) fluorescence microscope with an X-Cite 120 PC Q lamp and the images were analysed with NIS software.

Caspases 3/7 assay

The activity of caspases 3/7 on OVCAR-5 cancer cells was determined by Caspase-Glo™ 3/7 Assay (Cat. #G8091; Promega: Madison, WI, USA) following the standard protocol for cells cultured in a 96-well plate. 2000 cells per well were seeded on 96-well plates. After incubation overnight at 37 °C (5% CO_2), cells were treated at IC_{50} concentrations. After 3, 6, 24 and 48 hours of treatment, the caspase activation was measured with the Caspase-Glo™ 3/7 Assay with BioTek Synergy H1. Data are normalized to heathy cells for each time point.

Crystal structure determination

Data for crystals of **7-Br**, **7-Cl**, **4a**, **4a-Br**, **4a-Cl** and **6a** were collected at the XRD2 beamline of the Elettra Synchrotron, Trieste (Italy),[67] using a monochromatic wavelength of 0.620 Å, at 100 K or 298 K. The data sets were integrated, scaled, and corrected for Lorentz absorption and polarization effects using the XDS package.[68] The structures were solved by direct methods using the SHELXT program[69] and refined using full-matrix least-squares implemented in SHELXL-2019/3.[70] Thermal motions for all non-hydrogen atoms were treated anisotropically and hydrogen atoms were included at calculated positions, riding on their carrier atoms. Geometric restraints (DFIX, DANG, FLAT) were used to properly model disordered and poorly defined fragments. The Coot program was used for structure building.[71] Pictures were prepared using Ortep3[72] and Pymol[73] software. Crystal data are given in Table S1 in the ESI.† Crystallographic data were deposited with the Cambridge Crystallographic Data Centre and allocated the deposition numbers CCDC 2324443 (**6a** at 100 K), 2324442 (**4a** at 100 K), 2324438 (**4a-Br** at 298 K), 2324439 (**7-Cl** at 100 K), 2324440 (**7-Br** at 298 K) and 2324441 (**4a-Cl** at 298 K).†

Author contributions

Fabiano Visentin, Giovanni Tonon, Laura Orian, Flavio Rizzolio, Thomas Scattolin: conception and design of study; Giovanni Tonon, Matteo Mauceri, Rachele Piccolo, Claudio Santo, Nicola Demitri, Laura Orian, Pablo A. Nogara, João Batista T. Rocha: acquisition of data; Giovanni Tonon, Matteo Mauceri, Enrico Cavarzerani, Rachele Piccolo, Claudio Santo, Nicola Demitri, Laura Orian, Pablo A. Nogara, João Batista T. Rocha, Flavio Rizzolio, Fabiano Visentin and Thomas Scattolin: analysis and/or interpretation of data; Thomas Scattolin, Laura Orian, Giovanni Tonon, Flavio Rizzolio: project management, fund acquisition, writing, review, and editing.

Conflicts of interest

There are no conflicts to declare.

Acknowledgements

Funding: this research was funded by the Fondazione AIRC per la Ricerca sul Cancro, IG23566.

References

1 A. F. Littke and G. C. Fu, *Angew. Chem., Int. Ed.*, 2002, **41**, 4176.
2 J. F. Hartwig, *Angew. Chem., Int. Ed.*, 1998, **37**, 2046.
3 P. Ruiz-Castillo and S. L. Buchwald, *Chem. Rev.*, 2016, **116**, 12564.
4 C. Liu, H. Zhang, W. Shi and A. Lei, *Chem. Rev.*, 2011, **111**, 1780.
5 A. Brennführer, H. Neumann and M. Beller, *Angew. Chem., Int. Ed.*, 2009, **48**, 4114.
6 C. Valente, S. Çalimsiz, K. H. Hoi, D. Mallik, M. Sayah and M. G. Organ, *Angew. Chem., Int. Ed.*, 2012, **51**, 3314.
7 I. P. Beletskaya, F. Alonso and V. S. Tyurin, *Coord. Chem. Rev.*, 2019, **385**, 137.
8 S. E. Hooshmand, B. Heidari, R. Sedghi and R. S. Varma, *Green Chem.*, 2019, **21**, 381.
9 D. Shen, Y. Xu and S. Shi, *J. Am. Chem. Soc.*, 2019, **141**, 14938.
10 N. Angello, V. Rathore, W. Beker, A. Wołos, E. R. Jira, R. Roszak, T. Wu, C. M. Schroeder, A. Aspuru-Guzik, B. A. Grzybowski and M. D. Burke, *Science*, 2022, **378**, 399.
11 J. L. Bras and J. Muzart, *Chem. Rev.*, 2011, **111**, 1170.
12 A. Biffis, P. Centomo, A. Del Zotto and M. Zecca, *Chem. Rev.*, 2018, **118**, 2249.
13 I. P. Beletskaya and A. V. Cheprakov, *Chem. Rev.*, 2000, **100**, 3009.
14 D. Roy and Y. Uozumi, *Adv. Synth. Catal.*, 2018, **360**, 602.
15 R. Dorel, C. P. Grugel and A. M. Haydl, *Angew. Chem., Int. Ed.*, 2019, **58**, 17118.
16 M. M. Heravi, Z. Kheilkordi, V. Zadsirjan, M. Heydari and M. Malmir, *J. Organomet. Chem.*, 2018, **861**, 17.
17 D. T. Ahneman, J. G. Estrada, S. Lin, S. D. Dreher and A. G. Doyle, *Science*, 2018, **360**, 186.
18 C. Cordovilla, C. Bartolomé, J. M. Martínez-Ilarduya and P. Espinet, *ACS Catal.*, 2015, **5**, 3040.
19 Q. Zhao, G. Meng, S. P. Nolan and M. Szostak, *Chem. Rev.*, 2020, **120**, 1981.
20 F. Villalba and A. C. Albéniz, *Dalton Trans.*, 2022, **51**, 14847.
21 M. Yamashita, J. V. Cuevas-Vicario and J. F. Hartwig, *J. Am. Chem. Soc.*, 2003, **125**, 16347.
22 D. Kruis, B. A. Markies, A. J. Canty, J. Boersma and G. Van Koten, *J. Organomet. Chem.*, 1997, **532**, 235.
23 D. Barafiano and J. F. Hartwig, *J. Am. Chem. Soc.*, 1995, **117**, 2937.
24 Z. Zhu, C. D. Park, K. Klimes and J. Li, *Adv. Opt. Mater.*, 2019, **7**, 1801518.
25 J. Yang, X. Feng, N. Li, J. Li, X. Song, M. Li, G. Cui, J. Zhang, C. Jiang, C. Yang and K. Li, *Sci. Adv.*, 2023, **9**, eadh0198.

26 A. R. Kapdi and I. J. Fairlamb, *Chem. Soc. Rev.*, 2014, **43**, 4751.
27 C. Cullinane, G. B. Deacon, P. R. Drago, A. P. Erven, P. C. Junk, J. Luu, G. Meyer, S. Schmitz, I. Ott, J. Schur, L. K. Webster and A. Klein, *Dalton Trans.*, 2018, **47**, 1918.
28 J. Ruiz, N. Cutillas, C. Vicente, M. D. Villa, G. López, J. Lorenzo, F. X. Aviles, V. Moreno and D. Bautista, *Inorg. Chem.*, 2005, **44**, 7365.
29 T. Scattolin, V. A. Volonshki, F. Visentin and S. P. Nolan, *Cell Rep. Phys. Sci.*, 2021, **2**, 100446.
30 T. Scattolin, I. Pessotto, E. Cavarzerani, V. Canzonieri, L. Orian, N. Demitri, C. Shmidt, A. Casini, E. Bortolamiol, F. Rizzolio, F. Visentin and S. P. Nolan, *Eur. J. Inorg. Chem.*, 2022, e202200.
31 T. Scattolin, E. Bortolamiol, F. Visentin, S. Palazzolo, I. Caligiuri, T. Perin, V. Canzonieri, N. Demitri, F. Rizzolio and A. Togni, *Chem. – Eur. J.*, 2020, **26**, 1.
32 T. Scattolin, L. Canovese, N. Demitri, R. Gambari, I. Lampronti, C. Santo, F. Rizzolio, I. Caligiuri and F. Visentin, *Dalton Trans.*, 2018, **47**, 13616.
33 T. Scattolin, E. Bortolamiol, I. Caligiuri, F. Rizzolio, N. Demitri and F. Visentin, *Polyhedron*, 2020, **186**, 114607.
34 T. Scattolin, E. Bortolamiol, F. Rizzolio, N. Demitri and F. Visentin, *Appl. Organomet. Chem.*, 2020, e5876.
35 T. Scattolin, A. Piccin, M. Mauceri, F. Rizzolio, N. Demitri, V. Canzonieri and F. Visentin, *Polyhedron*, 2021, **207**, 115381.
36 A. Madabeni, T. Scattolin, E. Bortolamiol, F. Visentin and L. Orian, *Organometallics*, 2024, DOI: **10.1021/acs.organomet.3c00514**.
37 L. Fiebig, N. Schlörer, H. G. Schmalz and M. Schäfer, *Chem. – Eur. J.*, 2014, **20**, 4906.
38 D. Barañano and J. F. Hartwig, *J. Am. Chem. Soc.*, 1995, **117**, 2937.
39 E. Shirakawa and T. Hiyama, *J. Organomet. Chem.*, 1999, **576**, 169.
40 G. Mann, D. Barañano, J. F. Hartwig, A. L. Rheingold and I. A. Guzei, *J. Am. Chem. Soc.*, 1998, **120**, 9205.
41 L. Canovese, F. Visentin, C. Biz, T. Scattolin, C. Santo and V. Bertolasi, *Polyhedron*, 2015, **102**, 94.
42 T. Scattolin, F. Visentin, C. Santo, V. Bertolasi and L. Canovese, *Dalton Trans.*, 2016, **45**, 11560.
43 J. Kim, B.-K. Koo and J. A. Knoblich, *Nat. Rev. Mol. Cell Biol.*, 2020, **21**, 571.
44 (*a*) S. Palazzolo, M. Hadla, C. R. Spena, I. Caligiuri, R. Rotondo, M. Adeel, V. Kumar, G. Corona, V. Canzonieri, G. Toffoli and F. Rizzolio, *Cancers*, 2019, **11**, 1997; (*b*) C. Granchi, G. Bononi, R. Ferrisi, E. Gori, G. Mantini, S. Glasmacher, G. Poli, S. Palazzolo, I. Caligiuri, F. Rizzolio, V. Canzonieri, T. Perin, J. Gertsch, A. Sodi, E. Giovannetti, M. Macchia, F. Minutolo, T. Tuccinardi and A. Chicca, *Eur. J. Med. Chem.*, 2021, **209**, 112857; (*c*) F. Duzagac, G. Saorin, L. Memeo, V. Canzonieri and F. Rizzolio, *Cancers*, 2021, **13**, 1.
45 D. D. Bowtell, S. Böhm, A. A. Ahmed, P. J. Aspuria, R. C. Bast, V. Beral, J. S. Berek, M. J. Birrer, S. Blagden, M. A. Bookman, J. D. Brenton, K. B. Chiappinelli, F. C. Martins, G. Coukos, R. Drapkin, R. Edmondson, C. Fotopoulou, H. Gabra, J. Galon, C. Gourley, V. Heong, D. G. Huntsman, M. Iwanicki, B. Y. Karlan, A. Kaye, E. Lengyel, D. A. Levine, K. H. Lu, I. A. McNeish, U. Menon, S. A. Narod, B. H. Nelson, K. P. Nephew, P. Pharoah, D. J. Powell, P. Ramos, I. L. Romero, C. L. Scott, A. K. Sood, E. A. Stronach and F. R. Balkwill, *Nat. Rev. Cancer*, 2015, **15**, 668.
46 (*a*) R. Perets, G. A. Wyant, K. W. Muto, J. G. Bijron, B. B. Poole, K. T. Chin, J. Y. Chen, A. W. Ohman, C. D. Stepule, S. Kwak, A. M. Karst, M. S. Hirsch, S. R. Setlur, C. P. Crum, D. M. Dinulescu and R. Drapkin, *Cancer Cell*, 2013, **24**, 751; (*b*) S. J. Hill, B. Decker, E. A. Roberts, N. S. Horowitz, M. G. Muto, M. J. Worley, C. M. Feltmate, M. R. Nucci, E. M. Swisher, H. Nguyen, C. Yang, R. Morizane, B. S. Kochupurakkal, K. T. Do, P. A. Konstantinopoulos, J. F. Liu, J. V. Bonventre, U. A. Matulonis, G. I. Shapiro, R. S. Berkowitz, C. P. Crum and A. D. D'Andrea, *Cancer Discovery*, 2018, **8**, 1404; (*c*) O. Kopper, C. J. de Witte, K. Lõhmussaar, J. E. Valle-Inclan, N. Hami, L. Kester, A. V. Balgobind, J. Korving, N. Proost, H. Begthel, L. M. van Wijk, S. A. Revilla, R. Theeuwsen, M. van de Ven, M. J. van Roosmalen, B. Ponsioen, V. W. H. Ho, B. G. Neel, T. Bosse, K. N. Gaarenstroom, H. Vrieling, M. P. G. Vreeswijk, P. J. van Diest, P. O. Witteveen, T. Jonges, J. L. Bos, A. van Oudenaarden, R. P. Zweemer, H. J. G. Snippert, W. P. Kloosterman and H. Clevers, *Nat. Med.*, 2019, **25**, 838.
47 E. Smolle, V. Taucher and J. Haybaeck, *Anticancer Res.*, 2014, **34**, 1553.
48 E. Kipps, D. S. P. Tan and S. B. Kaye, *Nat. Rev. Cancer*, 2013, **13**, 273.
49 E. Cavarzerani, I. Caligiuri, M. Bartoletti, V. Canzonieri and F. Rizzolio, *Front. Bioeng. Biotechnol.*, 2023, **11**, 1135374.
50 M. Ott, J. D. Robertson, V. Gogvadze, B. Zhivotovsky and S. Orrenius, *Proc. Natl. Acad. Sci. U. S. A.*, 2002, **99**, 1259.
51 I. H. Ismail, T. I. Wadhra and O. Hammarsten, *Nucleic Acids Res.*, 2007, **35**, e36.
52 M. Fragkos, J. Jurvansuu and P. Beard, *Mol. Cell. Biol.*, 2009, **29**, 2828.
53 M. Brentnall, L. Rodriguez-Menocal, R. L. De Guevara, E. Cepero and L. H. Boise, *BMC Cell Biol.*, 2013, **14**, 32.
54 (*a*) A. Heydari and H. Mansouri-Torshizi, *RSC Adv.*, 2016, **6**, 96121; (*b*) K. Karami, M. Rafiee, Z. M. Lighvan, M. Zakariazadeh, A. Yeganeh-Faal, S. Esmaeili and A. A. Momtazi-Borojeni, *J. Mol. Struct.*, 2018, **1154**, 480.
55 (*a*) C. K. S. Pillai and U. S. Nandi, *Biochim. Biophys. Acta*, 1977, **474**, 11; (*b*) A. G. Tikhomirov, N. A. Ivanova, O. S. Erofeeva, L. B. Gorbacheva and I. A. Efimenko, *Russ. J. Coord. Chem.*, 2003, **29**, 489.
56 F. Neese, *Wiley Interdiscip. Rev.: Comput. Mol. Sci.*, 2017, **8**, e1327.
57 N. Mardirossian and M. Head-Gordon, *J. Chem. Phys.*, 2015, **142**, 074111.

58 F. Weigend and R. Ahlrichs, *Phys. Chem. Chem. Phys.*, 2005, **7**, 3297.
59 N. Mardirossian and M. Head-Gordon, *J. Chem. Phys.*, 2016, **144**, 214110.
60 O. Trott and A. J. Olson, *J. Comput. Chem.*, 2009, **31**, 455.
61 (*a*) R. A. Hussain, A. Badshah, M. Sohail, B. Lal and K. Akbar, *J. Mol. Struct.*, 2013, **1048**, 367; (*b*) A. Zianna, G. D. Geromichalos, A.-M. Fiotaki, A. G. Hatzidimitriou, S. Kalogiannis and G. Psomas, *Pharmaceuticals*, 2022, **15**, 886; (*c*) N. Shahabadi, L. Ghaffari, Z. Mardani and F. Shiri, *Biol. Trace Elem. Res.*, 2021, **200**, 1988–2000.
62 (*a*) C. Lee, W. Yang and R. G. Parr, *Phys. Rev. B: Condens. Matter Mater. Phys.*, 1988, **37**, 785; (*b*) A. D. Becke, *Phys. Rev. A*, 1988, **38**, 3098.
63 E. van Lenthe, E. J. Baerends and J. G. Snijders, *J. Chem. Phys.*, 1994, **101**, 9783.
64 (*a*) M. Bortoli, S. M. Ahmad, T. A. Hamlin, F. M. Bickelhaupt and L. Orian, *Phys. Chem. Chem. Phys.*, 2018, **20**, 27592; (*b*) M. Dalla Tiezza, F. M. Bickelhaupt and L. Orian, *ChemistryOpen*, 2019, **8**, 143; (*c*) M. Dalla Tiezza, F. M. Bickelhaupt and L. Orian, *ChemPhysChem*, 2018, **19**, 1766; (*d*) L. Orian, L. P. Wolters and F. M. Bickelhaupt, *Chem. – Eur. J.*, 2013, **40**, 12227; (*e*) L. Orian, M. Swart and F. M. Bickelhaupt, *ChemPhysChem*, 2014, **15**, 219; (*f*) A. Madabeni, M. Bortoli, P. A. Nogara, J. B. T. Rocha and L. Orian, *Inorg. Chem.*, 2021, **60**, 4646; (*g*) L. Orian, W.-J. van Zeist and F. M. Bickelhaupt, *Organometallics*, 2008, **27**, 4028.
65 (*a*) E. J. Baerends, D. E. Ellis and P. Ros, *Chem. Phys.*, 1973, **2**, 41; (*b*) G. te Velde, F. M. Bickelhaupt, E. J. Baerends, C. F. Guerra, S. J. A. van Gisbergen, J. G. Snijders and T. Ziegler, *J. Comput. Chem.*, 2001, **22**, 931.
66 (*a*) E. F. Pettersen, T. D. Goddard, C. C. Huang, G. S. Couch, D. M. Greenblatt, E. C. Meng and T. E. Ferrin, *J. Comput. Chem.*, 2004, **25**, 1605; (*b*) P. A. Nogara, F. B. Omage, G. R. Bolzan, C. P. Delgado, L. Orian and J. B. T. Da Rocha, *J. Mol. Model.*, 2022, **28**, 354.
67 A. Lausi, M. Polentarutti, S. Onesti, J. R. Plaisier, E. Busetto, G. Bais, L. Barba, A. Cassetta, G. Campi, D. Lamba, A. Pifferi, S. C. Mande, D. D. Sarma, S. M. Sharma and G. Paolucci, *Eur. Phys. J. Plus*, 2015, **130**, 1.
68 W. Kabsch, *Acta Crystallogr., Sect. D: Biol. Crystallogr.*, 2010, **66**, 125.
69 G. M. Sheldrick, *Acta Crystallogr., Sect. A: Found. Adv.*, 2015, **71**, 3.
70 G. M. Sheldrick, *Acta Crystallogr., Sect. C: Struct. Chem.*, 2015, **71**, 3.
71 P. Emsley, B. Lohkamp, W. Scott and K. Cowtan, *Acta Crystallogr., Sect. D: Biol. Crystallogr.*, 2010, **66**, 486.
72 L. Farrugia, *J. Appl. Crystallogr.*, 2012, **45**, 849.
73 L. Schrodinger, 2015, **https://www.pymol.org**.